JAERI-Research
99-067

EVALUATION OF STEAM GENERATOR U-TUBE INTEGRITY DURING PWR STATION BLACKOUT WITH SECONDARY SYSTEM DEPRESSURIZATION

December 1999

Akihide HIDAKA, Hideaki ASAKA, Shingo UENO*,
Takehito YOSHINO* and Jun SUGIMOTO

日本原子力研究所
Japan Atomic Energy Research Institute

本レポートは，日本原子力研究所が不定期に公刊している研究報告書です。
入手の問合わせは，日本原子力研究所研究情報部研究情報課（〒319－1195 茨城県那珂郡東海村）あて，お申し越しください。なお，このほかに財団法人原子力弘済会資料センター（〒319－1195　茨城県那珂郡東海村日本原子力研究所内）で複写による実費頒布をおこなっております。

This report is issued irregularly.
Inquiries about availability of the reports should be addressed to Research Information Division, Department of Intellectual Resources, Japan Atomic Energy Research Institute, Tokai-mura, Naka-gun, Ibaraki-ken 〒319－1195, Japan.

編集兼発行　日本原子力研究所

Evaluation of Steam Generator U-Tube Integrity during PWR Station Blackout with Secondary System Depressurization

Akihide HIDAKA, Hideaki ASAKA, Shingo UENO*, Takehito YOSHINO** and Jun SUGIMOTO+

Department of Reactor Safety Research
Nuclear Safety Research Center
Tokai Research Establishment
Japan Atomic Energy Research Institute
Tokai-mura, Naka-gun, Ibaraki-ken

(Received November 2, 1999)

In PWR severe accidents such as station blackout, the integrity of steam generator U-tube would be threatened early at the transient among the pipes of primary system. This is due to the hot leg countercurrent natural circulation (CCNC) flow which delivers the decay heat of the core to the structures of primary system if the core temperature increases after the secondary system depressurization. From a view point of accident mitigation, this steam generator tube rupture (SGTR) is not preferable because it results in the direct release of primary coolant including fission products (FP) to the environment. Recent SCDAP/RELAP5 analyses by USNRC showed that the creep failure of pressurizer surge line which results in release of the coolant into containment would occur earlier than SGTR during the secondary system depressurization. However, the analyses did not consider the decay heat from deposited FP on the steam generator U-tube surface.

In order to investigate the effect of decay heat on the steam generator U-tube integrity, the hot leg CCNC flow model used in the USNRC's calculation was, at first, validated through the analysis for JAERI's LSTF experiment. The CCNC model reproduced well the thermohydraulics observed in the LSTF experiment and thus the model is mostly reliable. An analytical study was then performed with SCDAP/RELAP5 for TMLB' sequence of Surry plant with and without secondary system depressurization. The decay heat from deposited FP was calculated by JAERI's FP aerosol behavior analysis code, ART. The ART analysis showed that relatively large amount of FPs may deposit on steam generator U-tube inlet mainly by thermophoresis. The SCDAP/RELAP5

analyses considering the FP decay heat predicted small safety margin for steam generator U-tube integrity during secondary system depressurization. Considering associated uncertainties in the analyses, the potential for SGTR cannot be ignored. Accordingly, this should be considered in the evaluation of merits and demerits of accident management measures related with the secondary system depressurization.

Keywords: Accident Mitigation, Steam Generator Tube Rupture, Hot Leg Countercurrent Flow, Fission Products, Station Blackout, Secondary System Depressurization, SCDAP/RELAP5 Code, LSTF Experiment, ART Code, Surry Plant

---

+ Office of Planning

* Mitsubishi Research Institute, Inc.

** Toshiba Advanced Systems Corporation

2次系減圧を伴うPWR電源喪失事故時における蒸気発生器伝熱管健全性評価

日本原子力研究所東海研究所安全性試験研究センター原子炉安全工学部
日高　昭秀・浅香　英明・上野　信吾*・吉野　丈人**・杉本　純+

（1999年11月2日受理）

電源喪失事故のようなPWRのシビアアクシデント中に2次系が減圧された状態で炉心温度が上昇すると、ホットレグ水平対向流により炉心の崩壊熱が一次系配管に運ばれ、蒸気発生器伝熱管の健全性が最初に脅かされる可能性がある。蒸気発生器伝熱管が先に破損すると核分裂生成物（FP）を含む1次冷却材が環境中に直接放出されることから、影響緩和の観点からは望ましくない。最近、米国原子力規制委員会（USNRC）が行ったSCDAP/RELAP5コードを用いた解析は、2次系が減圧された場合、1次冷却材が格納容器中に放出される加圧器サージラインのクリープ破損の方が蒸気発生器伝熱管破損（SGTR）よりも先に起きることを示した。しかしながら、その解析では伝熱管表面に沈着したFPからの崩壊熱を考慮していない。

そこで、FP崩壊熱が蒸気発生器伝熱管の健全性に与える影響を調べるため、まず、USNRCの解析で使用したホットレグ水平対向流モデルを原研のLSTF実験とその解析を通して検証した。その結果、同モデルはLSTF実験で観測された熱水力現象を適切に再現し、ほぼ信頼できることを確認した。次にSCDAP/RELAP5コードを用いて、Surry炉の電源喪失事故中に2次系減圧を行った場合と行わない場合について解析を行った。沈着したFPからの崩壊熱は原研のFPエアロゾル挙動解析コードARTを用いて別途計算し、熱泳動機構により蒸気発生器伝熱管の入口部に比較的多くのFPが沈着することを明らかにした。そのFP崩壊熱をSCDAP/RELAP5計算で考慮した場合、2次系減圧時の蒸気発生器伝熱管の健全性はかろうじて確保された。しかしながら、計算に含まれる不確実性を考慮すると、蒸気発生器伝熱管が最初に破損する可能性を排除できない。このことは、2次系減圧に関するアクシデントマネジメント方策の得失を評価する上で考慮しておく必要がある。

東海研究所：〒319-1195　茨城県那珂郡東海村白方白根2-4
+　企画室
*　（株）三菱総合研究所
**　東芝アドバンストシステム（株）

This is a blank page.

CONTENTS

目　次

List of Tables

List of Figures

This is a blank page.

1. INTRODUCTION

The Level 1 Probabilistic Safety Assessment (PSA) for PWRs has shown that an accident initiated from a total station blackout (TMLB') is one of the dominant sequences leading to severe core damage[1]. The PSA study also pointed out that this TMLB' sequence would result in High Pressure Melt Ejection (HPME), which may lead to a Direct Containment Heating (DCH) and early failure of Containment Vessel (CV). Since HPME and DCH could be prevented by the depressurization of the Reactor Coolant System (RCS) prior to the failure of Reactor Pressure Vessel (RPV), the intentional depressurization had been proposed as one of accident management measures to mitigate the high pressure sequences such as TMLB' sequence[2),3)].

However, recent studies by Idaho National Engineering and Environmental Laboratory (INEEL) and Sandia National Laboratories (SNL) have resolved the DCH issues for PWRs[4),5)] because a creep rupture at hot leg or pressurizer surge line would occur prior to the RPV meltthrough during TMLB' sequence mainly due to temperature increase by superheated steam delivered by a Counter-Current Natural Circulation (CCNC) at hot leg. As a result, the RCS could be depressurized successfully before the RPV meltthrough.

On the other hand, the secondary system depressurization is considered as one of accident management measures for PWR severe accidents with high pressure of primary system because it is expected that the heat removal due to flushing by depressurization would result in primary system depressurization followed by activation of high pressure injection system (HPI) or accumulator injection without loss of primary coolant. However, it was recently pointed out that if the core temperature increases after the secondary system depressurization, the integrity of Steam Generator (SG) U-tube would be threatened earliest among the pipes of primary system due to large pressure difference between primary and secondary systems, heat from superheated steam by hot leg CCNC flow and decay heat from deposited Fission Products (FP). From a view point of accident mitigation, the failure of hot leg or pressurizer surge line earlier than that of SG U-tube is preferable because the Steam Generator Tube Rupture (SGTR) results in the direct release of primary coolant including FP to the environment.

Moreover, a representative analysis[1)] for Surry plant showed that a containment bypass frequency (associated with severe accident-induced tube failure) is approximately 3.9×10^{-6} per reactor year and 60 % of the bypass frequency is attributed to temperature-induced SGTR (2.4×10^{-6} / RY). Since the frequency of SGTR is not small and cannot be ignored, it is important to

evaluate in detail the SG U-tube integrity during severe accidents.

Recent SCDAP/RELAP5[6] analyses by USNRC showed that the hot leg CCNC flow would result in the failure of hot leg or pressurizer surge line earlier than SGTR during the secondary system depressurization[7]. However, the analyses did not consider the decay heat from deposited FP on SG U-tube surface. In order to investigate the effect of decay heat on the SG U-tube integrity, analytical studies were performed by using the SCDAP/RELAP5/Mod3.1 with the hot leg CCNC flow model for a total station blackout (TMLB') sequence of Surry nuclear plant with and without secondary system depressurization. Before the analysis, the hot leg CCNC flow model which was originally prepared by INEEL was validated by applying it to the JAERI's Large Scale Test Facility (LSTF) experiment[8]. The decay heat from deposited FP was calculated by JAERI's FP aerosol behavior analysis code, ART[9] and the calculated decay heat was reflected on the thermohydraulic and thermal response analyses with SCDAP/RELAP5.

This report summarizes the validation results of the INEEL's hot leg CCNC model through the analysis for LSTF experiment and the evaluation results of SG U-tube integrity during station blackout with and without the secondary system depressurization in the case that the hot leg CCNC flow and the decay heat from deposited FPs are taken into account.

2. HOT LEG COUNTERCURRENT FLOW

The natural circulation in RCS during severe accidents is identified as an important process that could impact the progression of severe accidents[1]. It is considered that during PWR severe accidents, three flow patterns of steam natural circulation as shown in **Fig. 2.1** could occur in RCS[6),10].

1) Full loop natural circulation
2) In-vessel natural circulation
3) Hot leg countercurrent natural circulation (CCNC)

The full loop natural circulation flow of steam could be caused mainly by the driving force due to heat generation at core and heat removal at SG U-tube. The in-vessel natural circulation flow of steam could be caused by the fuel relocation followed by formation of hollow space at upper part of core and the heat generation from debris bed or molten pool. The hot leg CCNC flow can

develop in the ex-vessel piping of PWRs with steam generator U-tube during severe accidents.

The hot leg CCNC flow in the ex-vessel piping is characterized by the flow of hot steam from the reactor vessel to the SG outlet plenum through the top of the hot leg pipe and a fraction of the SG U-tubes. The cooler steam then returns to the vessel through the remaining U-tubes and the bottom of the hot leg pipe as shown in **Fig. 2. 1**. The experiments with a one-seventh scale model of a Westinghouse PWR using water and sulfer hexafluoride (SF_6) showed that relatively stable hot leg CCNC flow patterns will develop during severe accidents[11]. In order to simulate this hot leg CCNC flow, a special nodalization (see **Fig. 4. 5**) for SCDAP/RELAP5 which is a one dimensional thermal hydraulic code was prepared originally by INEEL based on the calculation with a three-dimensional fluid dynamic code, COMMIX[12] for the Westinghouse one-seventh scale experiments. The detailed descriptions are in Chapter 4.

The hot leg CCNC flow plays an important role in many severe accident analyses because it can transfer energy from the core to other parts of RCS. As a results, RCS pressure boundaries will be heated and core damage progression can be affected. In TMLB' sequence of Surry plant, a calculation considering the hot leg CCNC flow predicts about 2,000 s delay of fuel cladding failure compared with the calculation without hot leg CCNC flow because the hot leg CCNC flow enhances the heat transfer from the core to steam at an early stage of core heatup and as a result, the fuel cladding heatup can be delayed. On the other hand, consideration of CCNC flow would result in higher temperature of hot-leg at a late phase of TMLB' sequence than that without hot leg CCNC flow because the hot leg CCNC flow, on the contrary, could enhance the heat transfer from high temperature core to the hot leg structure by superheated steam flow[13].

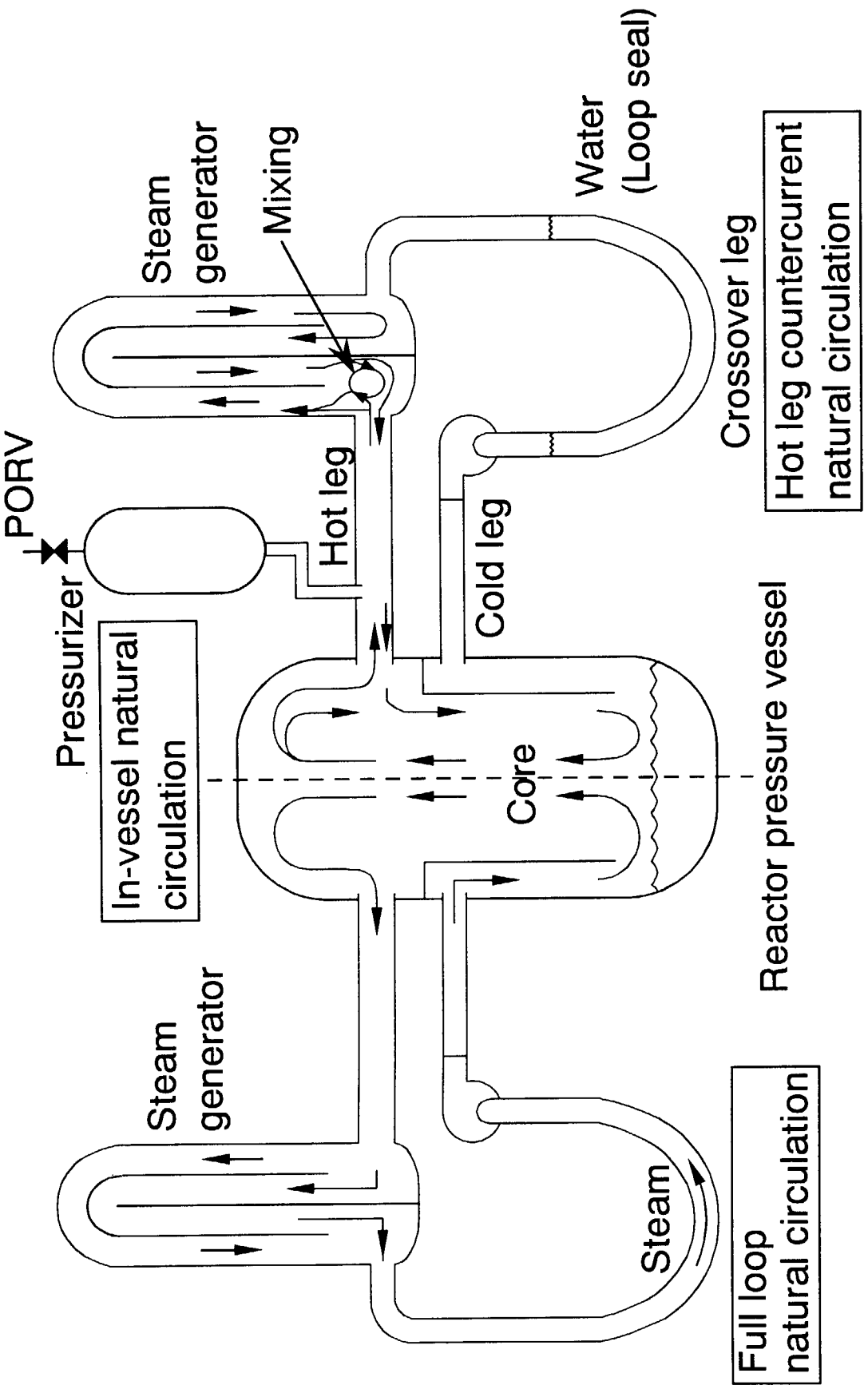

Fig.2.1 Natural circulation flow patterns developed during PWR severe accidents

3. ANALYSIS OF LSTF EXPERIMENT

Before the analysis of SG U-tube integrity with SCDAP/RELAP5, the hot leg CCNC flow model which was originally prepared by INEEL was validated by applying it to the JAERI's Large Scale Test Facility (LSTF) experiment (ST-NC-18) which simulated the hot leg CCNC flow during PWR severe accidents.

3.1 Experimental Facility

The ROSA-V Large Scale Test Facility (LSTF) is a 1/48 volumetric scaled, fully height, full-pressure model of a 4-loop (3,423 MWth) PWR[8]. A schematic of the LSTF is shown in **Fig.3.1**. The four primary loops of the reference PWR are represented by two equal-volume (2/48 scale) loops. The maximum heat transfer rate is designed as 35 MW per one SG (2/48 scaled value of one PWR SG). Each SG has scaled atmospheric relief valves (ARVs) to simulate the secondary-side pressure response in the reference PWR.

The core consists of 1,064 simulated fuel rods which are heated electrically at a maximum power of 10 MW. The rod diameter and pitch, the length of the heated zone (3.66 m), and the number of spacers are the same as those of a typical PWR. The axial core power profile is a 9-step chopped cosine with a peaking factor of 1.495. Flow paths at the core upper end are geometrically similar to the reference PWR end boxes and upper core support plate. Major design characteristics of the LSTF are compared with those of a typical PWR in **Table 3.1**.

3.2 Experimental Conditions

The experiment analyzed in the present analysis is designated as "ST-NC-18" test which was conducted on October 27, 1998 to simulate the hot leg countercurrent natural circulation (CCNC) flow during PWR severe accidents. Since the maximum core temperature of LSTF is 923K (trip temperature), the primary system pressure was decreased from 15.6 to 8.0 MPa and the saturation temperature was decreased less than 568 K to obtain large degree of superheat at upper plenum and hot leg piping. In the Westinghouse one-seventh scale experiment, water and sulfer hexafluoride (SF_6) were used as the coolant because SF_6 has the similar thermal properties at low temperature as those of superheated steam at high temperature. However, use of SF_6 was not allowed in the present LSTF experiment because SF_6 corrodes the copper electrode of the LSTF core.

The secondary side of steam generator-A was drained and isolated at the pressure of 8.0 MPa before the experiment initiation. The water level of secondary side of steam generator-B was set at 0.5 m high. The test initial steady state was established for a primary system pressure of 8.0 MPa and the saturation temperature of 568 K. After that, water of primary system was gradually drained. At the same time, the core power was adjusted so that the primary system might not be depressurized. The primary system drain was stopped when the core uncovery occurred and the degree of superheat at upper plenum exceeded 50 K. The experiment was continued by keeping the degree of superheat as much as possible under the condition of the core temperature lower than 923 K. The heat removal from the primary and secondary systems during the experiment was dominated by the natural heat radiation into containment atmosphere.

3.3 Analytical Methods

Since the maximum core temperature is 923 K in the LSTF experiment and it is not necessary to analyze the core degradation process, the SCDAP/RELAP5 code which can treat both of thermohydraulics and core degradation process during severe accidents was not used and instead only the one-dimensional thermohydraulic analysis code, RELAP5/Mod3[14] was used in the present analysis. It is noted that SCDAP/RELAP5/Mod3.1 used in the present study was prepared by combination of SCDAP, TRAP-MELT2[15] and RELAP5/Mod3. The RELAP5 nodalization for the LSTF experiment is shown in **Fig.3.2**. In the present analysis, calculations were performed from the onset (time = 0) of steam superheating at upper plenum of the core and was continued up to 6,600 s.

The pressure vessel was modeled with a downcomer, two channels in the core and upper plenum. RCS was modeled as two coolant loops individually with a lot of heat structures. The loop A has a pressurizer. The outer surface of the LSTF primary and secondary systems is assumed not to be adiabatic while adiabatic for those of the Surry RCS prepared by INEEL.

In order to simulate the hot leg countercurrent natural circulation (CCNC) flow and to validate the Surry hot leg CCNC model prepared originally by INEEL, a special nodalization was prepared for loop B at JAERI. It is noted that the Surry hot leg CCNC model was prepared based on the calculation with a three-dimensional fluid dynamic code, COMMIX for the Westinghouse one-seventh scale experiments on natural circulation.

In the hot leg CCNC flow model for the LSTF experiment, the similar flow volumes and flow areas as in the Surry input deck (see **Fig.4.4**) were used although they were reevaluated taking into account the 1/48 volumetric scale of the LSTF facility. The hot leg was divided into upper and lower halves. The SG inlet plenum was divided into three volumes to allow for the plenum mixing of hot and cold flow streams. The SG U-tube was divided into two volumes to carry cold and hot flow streams. While this model is used, a loop seal is usually made at the cross over leg and therefore most of steam flows backward at the SG outlet and goes back to the lower hot leg through the SG U-tube. It is noted that all the loss coefficients of SG plenum junction were reevaluated by trial and errors as used in the Surry CCNC model preparation so that the rate of mixing at SG inlet plenum and the SG circulation flow rates between the SG inlet and outlet plenums might agree well with those predicted in the Surry calculation (see **Fig.3.11** and **Fig.3.12**).

3.4 Experimental and Analytical Results

Measured and calculated total core power is shown in **Fig.3.3**. The calculated results were estimated from the total heat transfer rates from the surface of electric heaters to coolant. The calculation slightly underestimated before the hot leg CCNC flow was established at about 2,000 s because in the experiment, water of primary system continued to be drained before that while the calculation did not consider it. However, after 2,000 s, the calculation mostly agreed with the measured electrical power. The heat losses from primary and secondary systems are shown in **Fig.3.4**. These heat losses were caused mainly by the natural heat convection from the outer surface of primary and secondary systems into containment atmosphere. The heat transfer rate from primary to secondary system is equal to that at U-tube in Steam Generator-B and it corresponds mostly to the heat loss from the secondary system.

The pressurizer pressure is shown in **Fig.3.5**. The calculation mostly agrees with the experimental data. The steam temperature of the core upper plenum (volume 136) and its saturation temperature are shown in **Fig.3.6**. The superheating of steam in volume 136 began at 0 s and 50 K of superheating was achieved at about 2,000 s. The steam temperatures in the cross section of hot leg (volumes 206 and 260-3) are shown in **Fig.3.7**. The measured location for temperatures of superheated steam at upper and lower hot legs were at 30 mm inside, respectively from the inner surface of hot leg with 207 mm in diameter. On the other hand, the thermal boundary layer thickness, δt in which the thermal gradient in gas exists is given as follows:

$$\delta t = D / Nu = \lambda / h \qquad (3.1)$$

where D: representative length; diameter in case of pipe (m),
h: heat transfer coefficient ($W/m^2/K$),
Nu: Nusselt number (-),
λ: thermal conductivity (W/m/K).

The calculated thermal boundary layer thicknesses at upper and lower hot legs are equal to approximately 20 and 10 mm, respectively. Therefore, it is considered that the measured points were not located inside of the thermal boundary layer and therefore calculated steam temperature can be compared with the measured ones. It can be seen that the calculated temperatures of superheated steam at upper and lower hot legs agree well with the measurement. The steam mass flow rates at upper and lower hot legs are shown in **Fig.3.8**. The hot leg CCNC flow was mostly established at about 2000 s and the developed mass flow rate was equal to 0.1 kg/s. The flow rate at lower hot leg was slightly smaller than that at upper hot leg due to small amount of condensation at SG U-tube.

The steam mass flow rates with and without mixing at outlet of upper hot leg are shown in **Fig.3.9**. The calculation showed that about 86.5 % of the flow from the upper hot leg goes into the SG inlet plenum mixing volume 212 (see **Fig.3.8**) and the remaining 13.5 % flow passes through the inlet plenum without mixing (go into volume 270) as in the Surry calculation. The steam mass flow rates with and without steam generator circulation between inlet and outlet plenums are shown in **Fig.3.10**. The steam circulation flow between the inlet and outlet plenum of steam generator through U-tube was established after 2,000 s when the degree of steam superheating at the upper plenum of the core reached 50 K. The steam generator circulation flow which corresponds to about 80 % of upper hot leg steam mass flow was added at the steam generator U-tube inlet to the upper hot leg mass flow. These results coincide with those calculated by the Surry hot leg CCNC flow model.

The steam generator nodalization of Surry nuclear plant for a typical countercurrent simulation in terms of the total flow in the top of the hot leg (designated 'w') is shown in **Fig.3.11**. According to NUREG/CR-6150, Rev.1[6], 86.5% of the steam flow from the upper hot leg should go into the SG inlet plenum mixing volume 406 (see **Fig.4.4**) and the remaining 13.5 % flow should pass through the inlet plenum without mixing (go into volume 405). The SG U-tube was divided so that 35 % of the tubes were available to carry hot flow in the forward direction and

the remaining 65 % were available for cold flow in the backward direction. These values were evaluated by SCDAP/RELAP5 with the hot leg countercurrent flow model which was prepared based on the COMMIX calculation for 1/7 scale Westinghouse experiment with SF_6 instead of steam.

On the other hand, corresponding figure for the present analysis of the LSTF experiment is shown in **Fig.3.12**. It is noted that the ratio of steam mass flow rate at each junction to the total flow in the top of the hot leg corresponds to the calculated results at 4,000 s. The modification of loss coefficients at each junction in the LSTF calculation resulted in a good agreement of steam mass flow rate with the Surry calculation within the error of 10 %.

3.5 Evaluation of Surry Hot Leg Countercurrent Natural Circulation Model

For exact and detailed evaluation of Surry hot leg CCNC model, a three-dimensional thermohydraulic calculation should have been performed at first for the LSTF experiment as in the INEEL method and the hot leg CCNC model be prepared based on the calculation. However, in the present study, the CCNC flow model for the LSTF experiment was prepared based directly on the volumes modeled in the Surry input deck. Moreover, there was a difficulty for evaluation of the CCNC model. In the LSTF experiment, coolant mass flow rate can be measured by using the Pitot tubes. However, they had been broken and were not available in the present experiment. Therefore, the adequacy of the hot leg CCNC flow model had to be judged mainly from a comparison of steam and wall temperatures between calculation and measurement.

Although there were some insufficient matters as described in the above in the present method for the model evaluation, as shown in **Fig.3.7**, the calculation with the LSTF hot leg CCNC model could reproduce well the difference in measured steam temperature between upper and lower hot leg cross section. Moreover, the calculation could predict well the thermohydraulics of other reactor coolant systems and overall tendencies observed in the experiment. Accordingly, it can be concluded that the hot leg CCNC flow model for the Surry plant prepared by INEEL can be also applied to the LSTF experiment although the detailed should be reviewed more carefully based on the three-dimensional thermohydraulic calculation. In other words, it was confirmed that the Surry hot leg CCNC flow model is mostly reliable and can be applied to the CCNC issues.

However, the following points were also identified as important uncertainties through the present analysis by using the hot leg CCNC flow model.

1) Loss coefficients of SG plenum junction; In the case that the same flow volumes, junctions and loss coefficients as those in the Surry input deck were used for input deck of the LSTF experiment, the calculated flow pattern became slightly different from that in the Surry calculation. The possible main reason is due to the 1/48 volumetric scale of the LSTF facility. Therefore, before the present calculation, all the loss coefficients of SG plenum junctions were reevaluated by trial and errors as used in the Surry CCNC model preparation so that the similar steam mass flow rates at each junction as the Surry calculation might be obtained. The adequacy of these modified loss coefficients should be reevaluated based on the detailed three-dimensional thermohydraulic calculation for the LSTF experiment.

2) Mixing at inlet plenum of steam generator; It was pointed out in the USNRC's calculation that steam mixing at the inlet plenum of steam generator is one of important uncertainties. Our sensitivity studies showed that the ratio of steam mass flow rates with and without mixing at the inlet plenum of steam generator does not affect so much the overall tendencies of the hot leg CCNC flow pattern. For example, a sensitivity calculation with the condition of 50 % mixing / no mixing at the SG inlet plenum also showed that the calculated steam temperatures in the cross section of hot leg mostly agreed with the measurement. This fact suggests that a different ratio, for example, more than 13.5 % of upper hot leg steam flow could have passed through the inlet plenum without mixing and gone directly into the SG U-tube in the LSTF experiment.

Table 3.1 Major characteristics of LSTF

	LSTF	PWR[1)]	PWR/LSTF
Fluid volume (m^3)	7.23	347.0	48.0
Number of fuel rods	1,064	50,952	48
Core height (m)	3.66	3.66	1.0
Hot leg diameter D(m)	0.207	0.737	3.56
Length L (m)	3.69	6.99	1.89
$L/D^{0.5}$ ($m^{0.5}$)	8.15	8.15	1.0
Volume(m^3)	0.124	2.98	24.0
Number of loops	2	4	2
Number of SG U-tubes	141	3,382	24
Inner diameter of U-tube (mm)	19.6	19.6	1.0
Outer diameter of U-tube (mm)	25.4	22.23	1/1.14
Pitch of U-tubes (mm)	32.5	32.5	1.0
Average length of SG U-tube (m)	20.2	20.2	1.0

1) Typical Japanese-built 4-loop PWR (LSTF reference PWR)

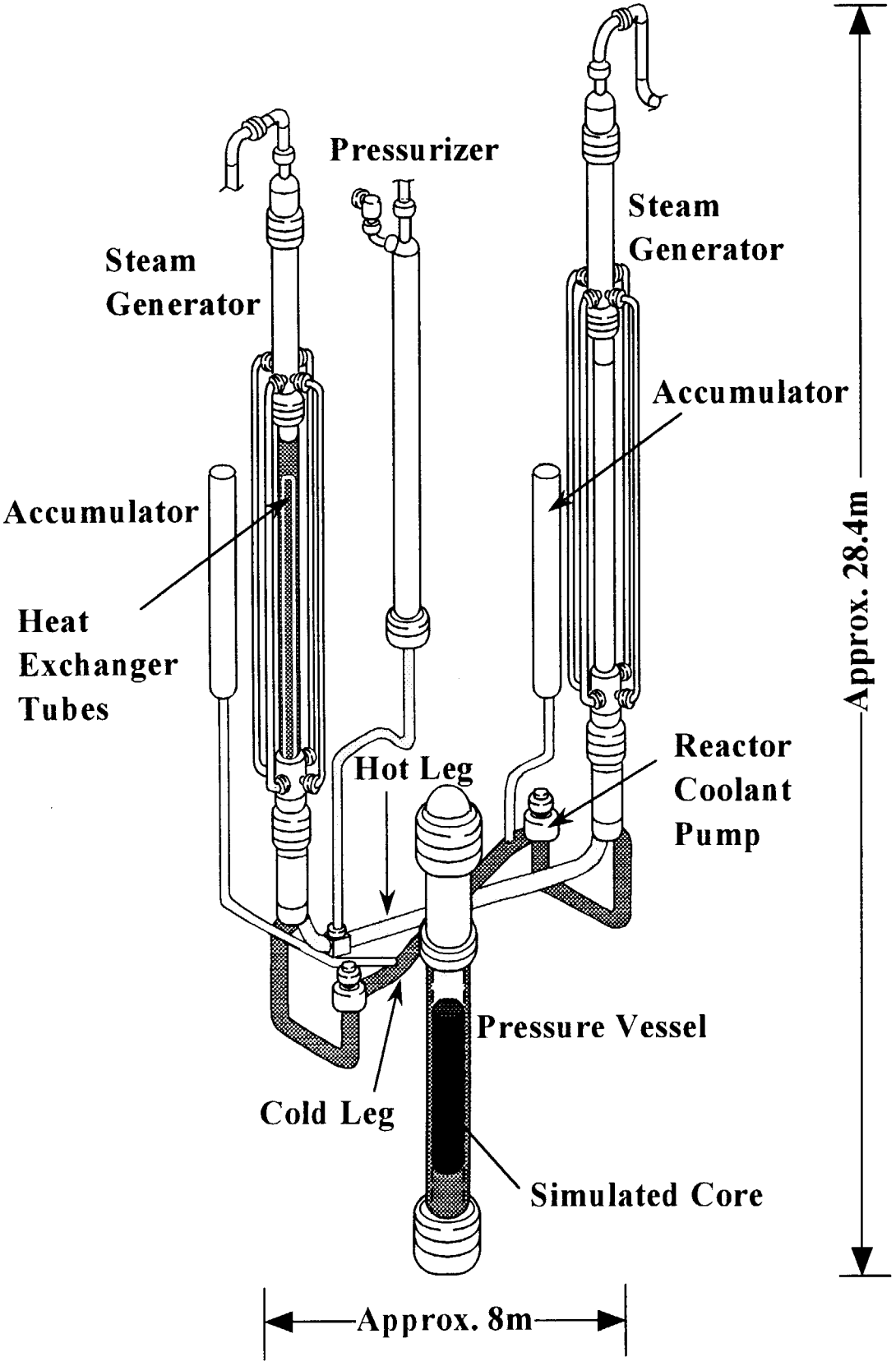

Fig. 3.1 Schematic of ROSA-V Large Scale Test Facility (LSTF)

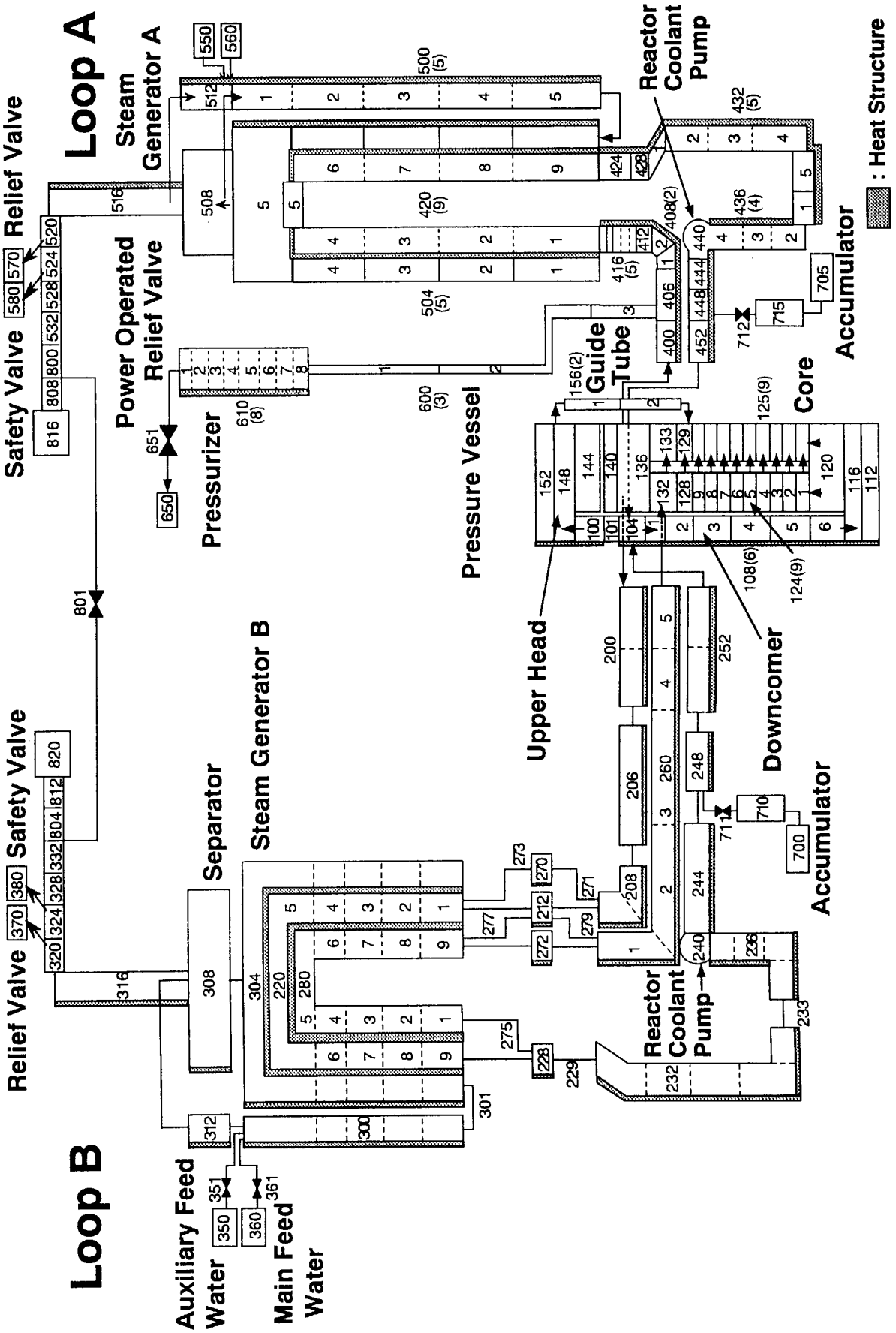

Fig.3.2 RELAP5 nodarization model for LSTF

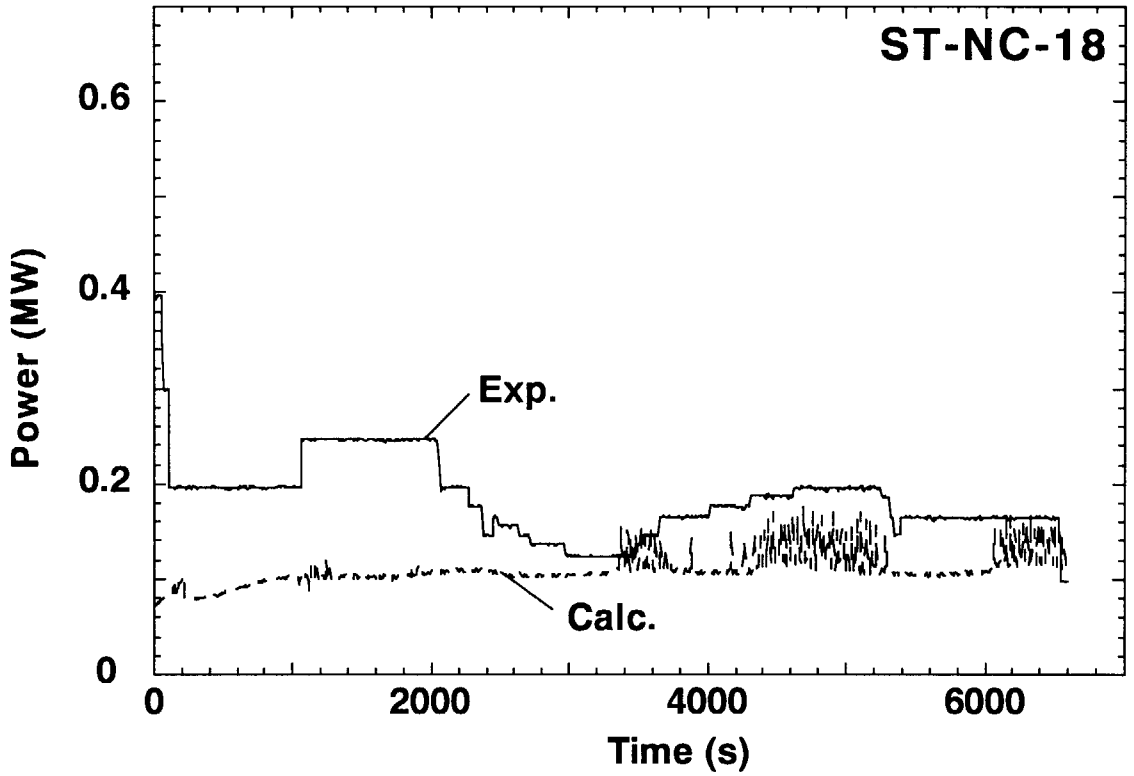

Fig.3.3 Total core power

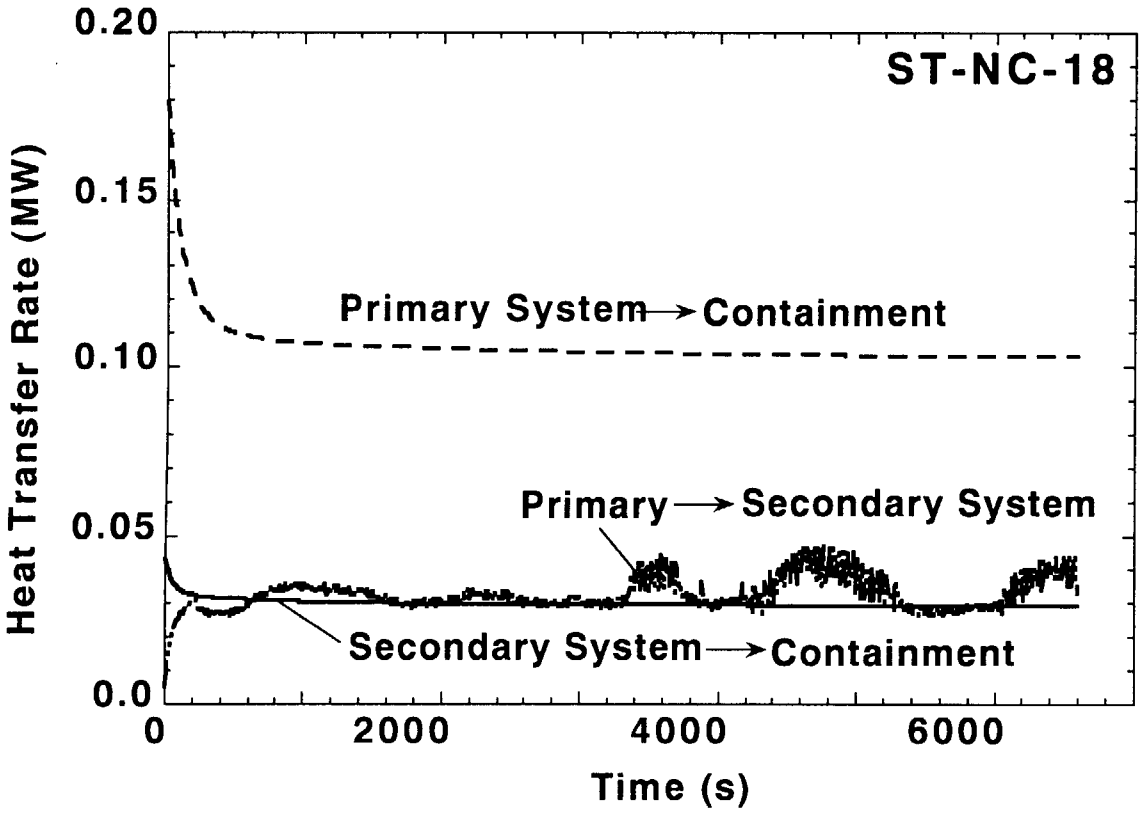

Fig.3.4 Heat losses from primary and secondary systems

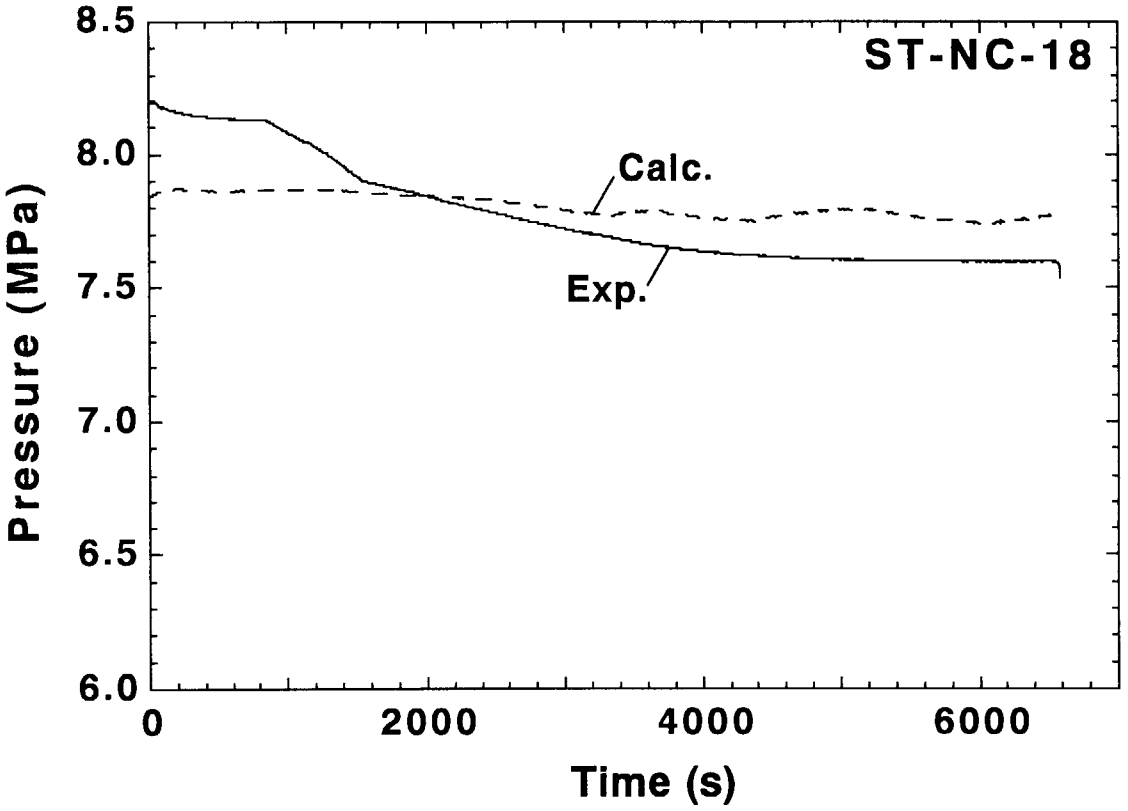

Fig.3.5 Pressurizer pressure

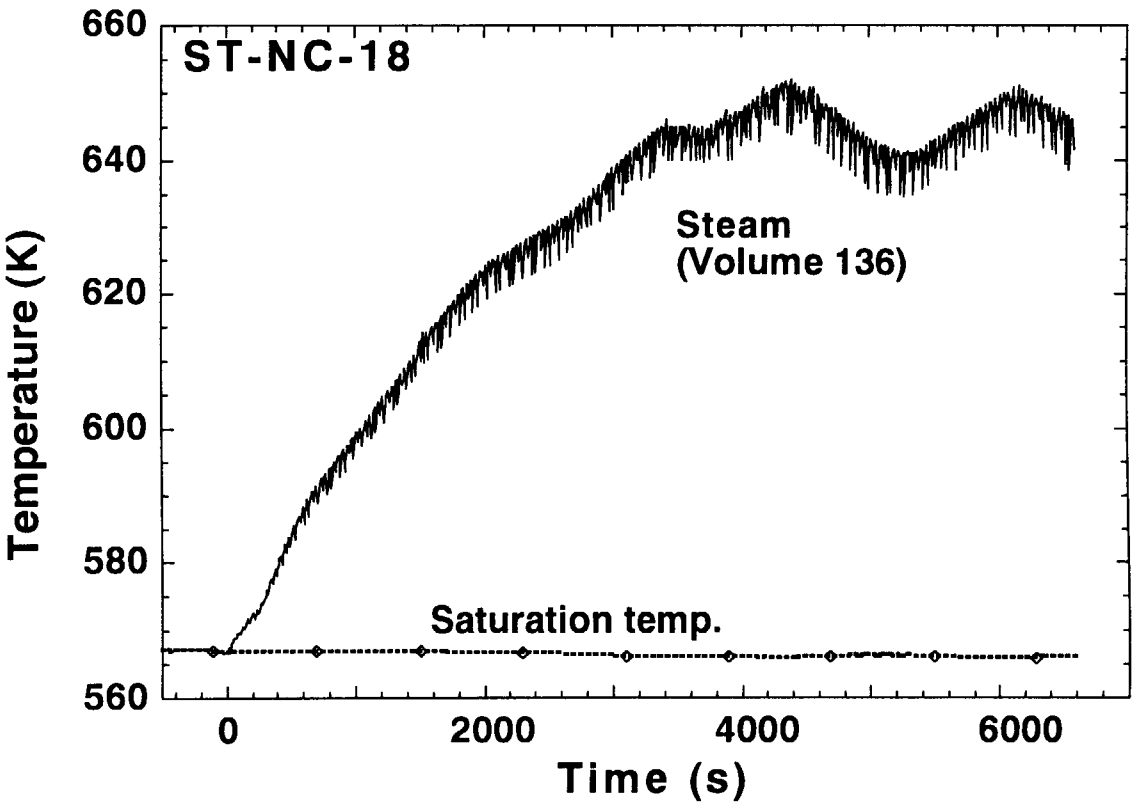

Fig.3.6 Steam temperature of core upper plenum

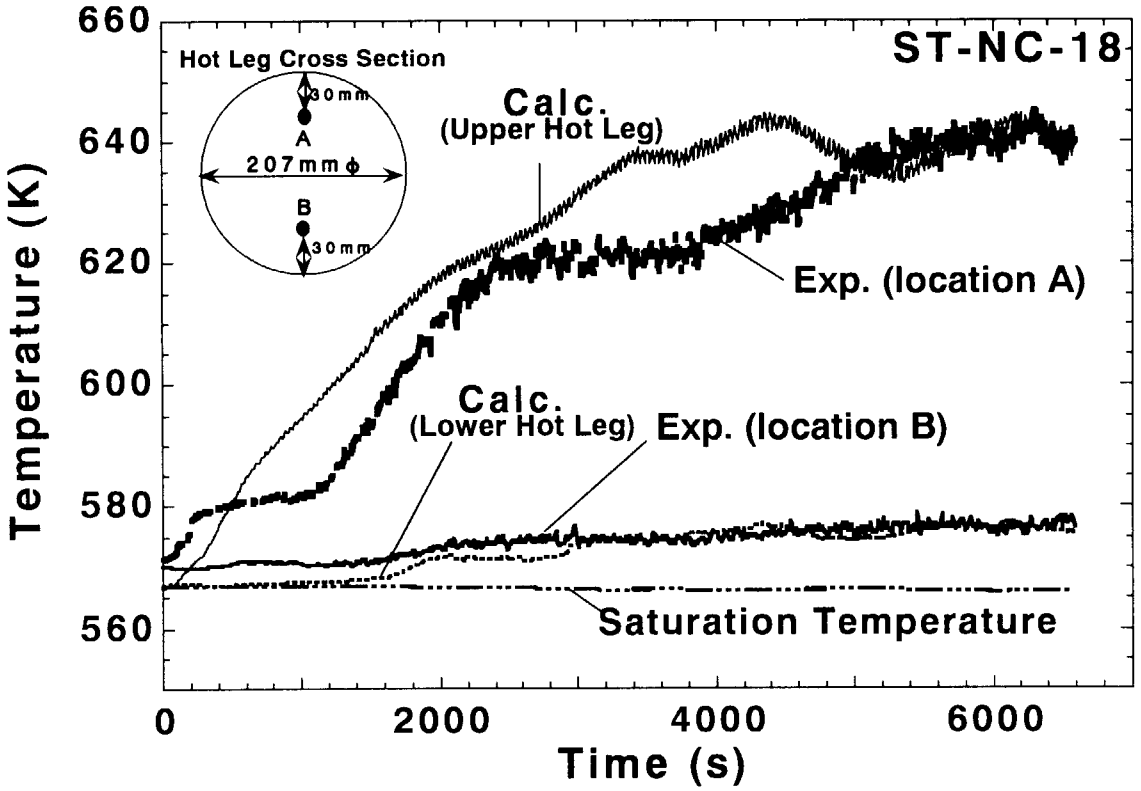

Fig.3.7 Temperature distribution in hot leg cross section

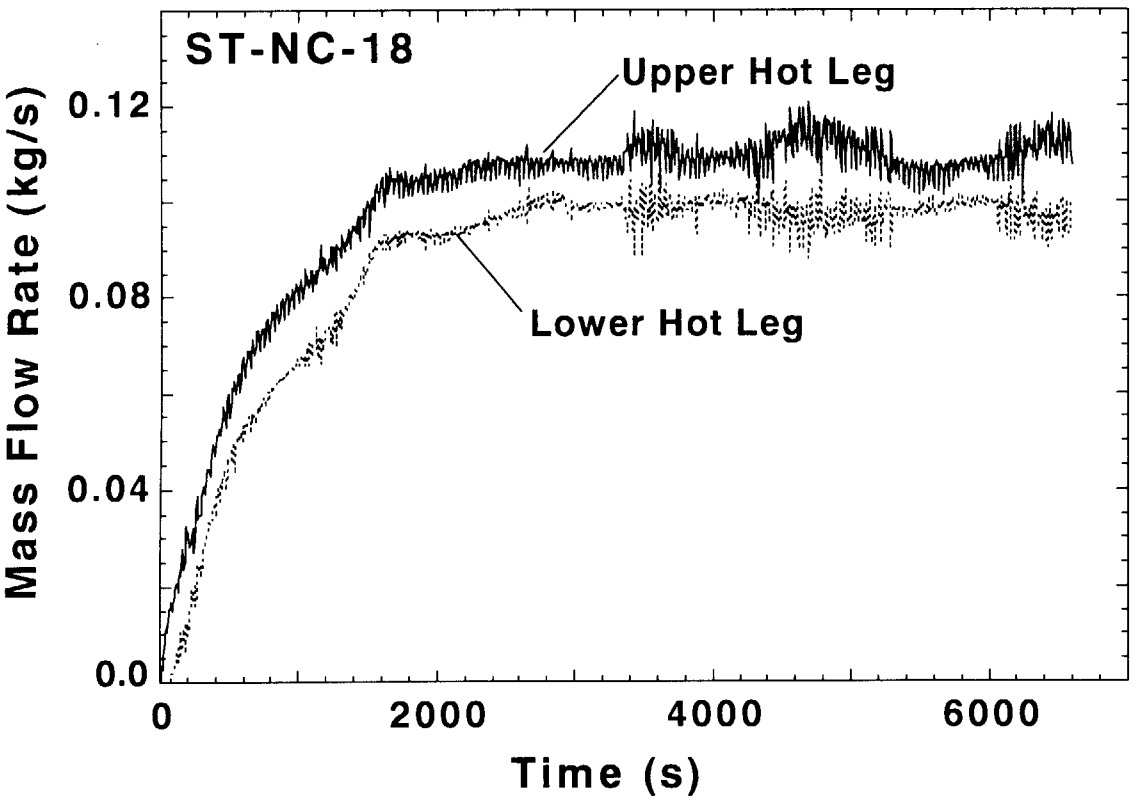

Fig.3.8 Steam mass flow rates at upper & lower hot legs

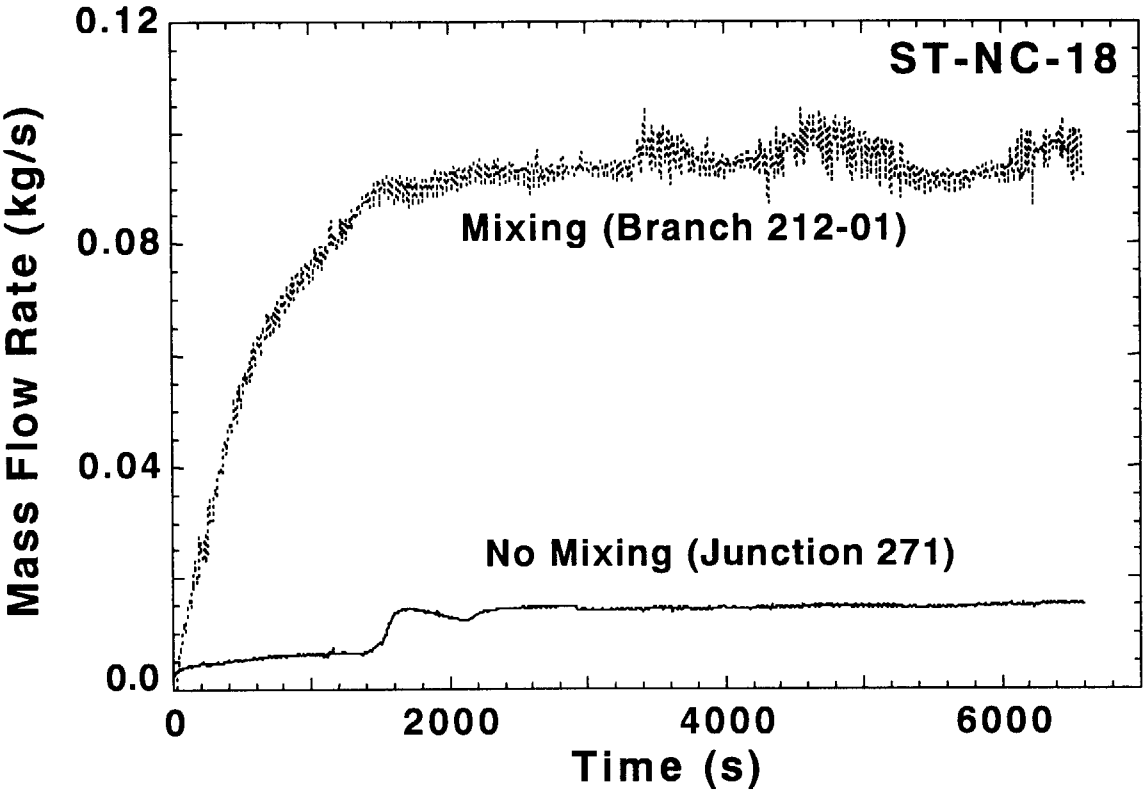

Fig.3.9 Steam mass flow rates with and without mixing at SG inlet plenum

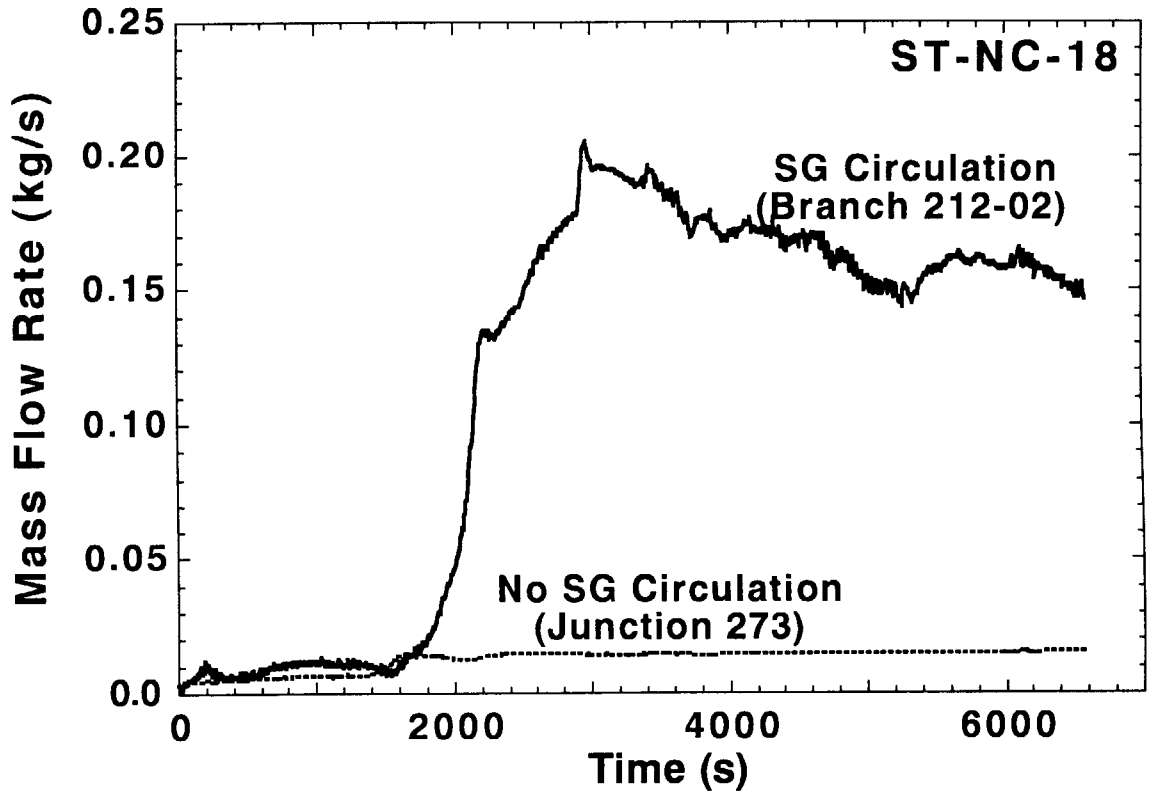

Fig.3.10 Steam mass flow rates with and without SG circulation between inlet and outlet plenums

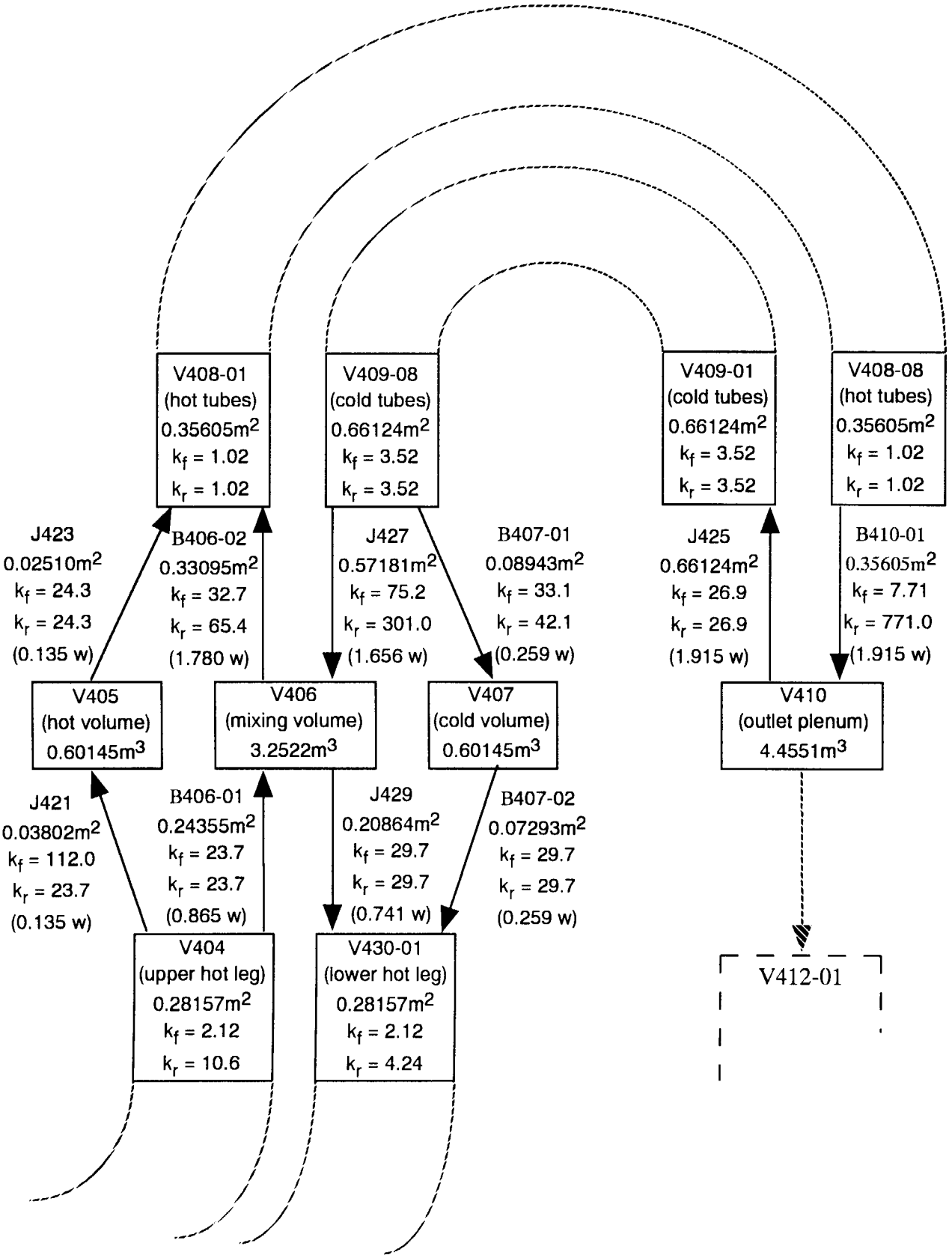

Fig.3.11 Surry SG nodalization for a typical countercurrent simulation in terms of the total flow in the top of the hot leg (designated 'w')

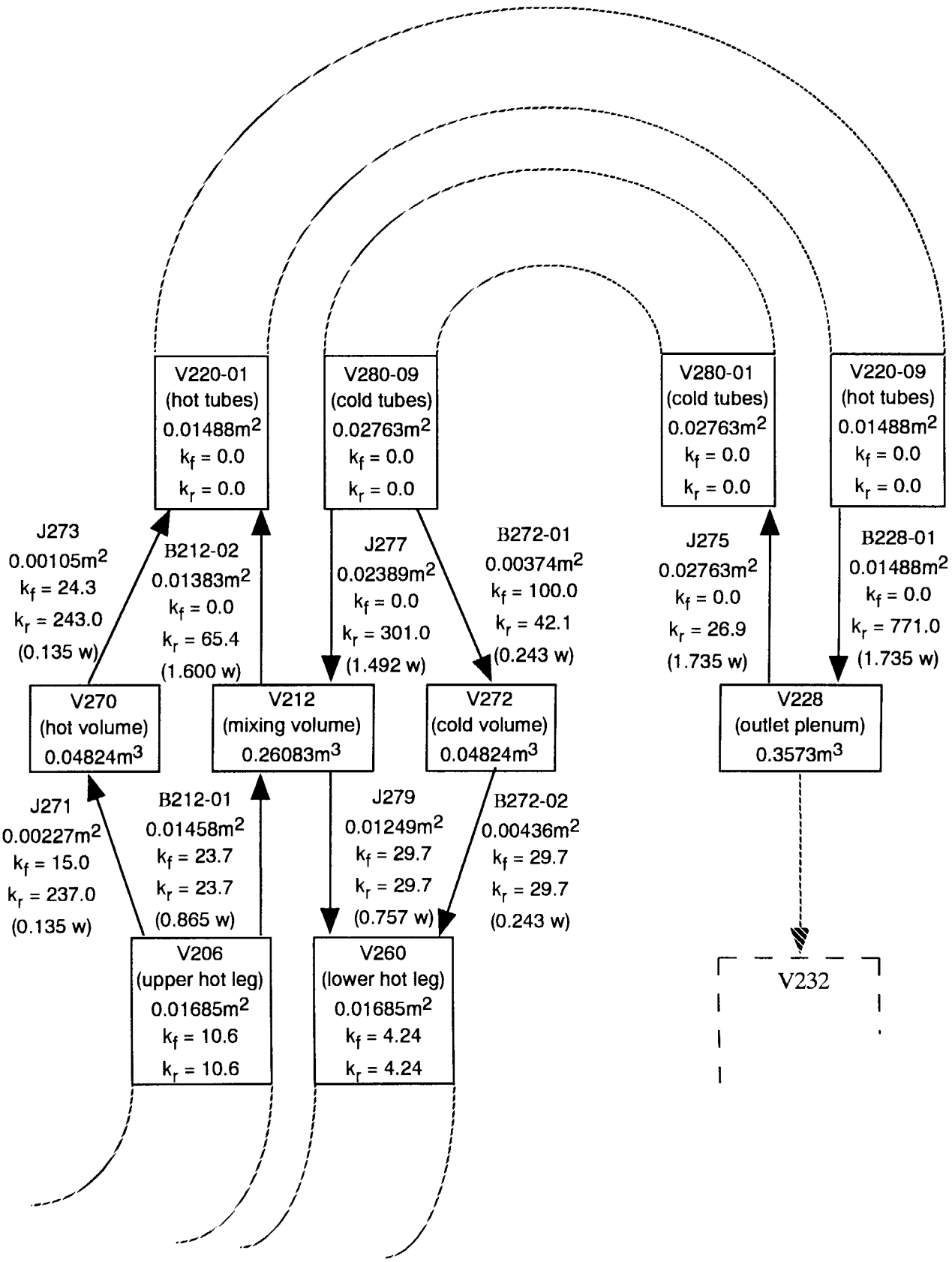

Fig.3.12 LSTF SG nodalization for a typical countercurrent simulation in terms of the total flow in the top of the hot leg (designated 'w')

4. ANALYSIS OF STEAM GENERATOR U-TUBE INTEGRITY DURING PWR STATION BLACKOUT

4.1 Reference Plant and Computer Codes

The reference plant is Surry nuclear power plant, a Westinghouse designed 3 loop PWR with a rated core thermal power of 2,441 MW[16]. The pressurizer is equipped with two Power Operated Relief Valves (PORVs). They open at 16.20 MPa and close at 15.72 MPa. The High Pressure Injection (HPI) and accumulator injection are initiated at the primary system pressure below 10.3 and 4.24 MPa, respectively. Each SG secondary has one Main Steam Relief Valve (MSRV) with flow area equal to 4.16×10^{-3} m^2 (47.0 kg/s of saturated liquid at 72.4 MPa).

The computer code used for FP deposition analysis was ART (Analysis of Radionuclide Transport)[9] code which is a module of JAERI's source term analysis code, THALES-2[9]. The types of physical processes modeled in ART are shown in **Fig. 4.1**. The code considers removal of radionuclides by natural deposition and engineered safety features (ESF). Aerosol growth by agglomeration and condensation or evaporation of volatile material at the aerosol surface are included. The code is capable of treating up to 60 materials including chemical compounds and of representing the systems by an arbitrary number of volumes. In each volume, materials can take the forms of gas, aerosol, deposition onto structure, and solution in water. The code solves the governing equations for multi-component aerosol and gaseous radionuclides. The "sectional method" developed by Gelbard et al.[17] is used to describe the size distribution of aerosols. The phase change of chemical species can be considered while the chemical reactions among FP elements in gas phase is not taken into account. ART has a fast running capability for application to Probabilistic Safety Assessment (PSA).

The thermohydraulic and structural response analyses was performed with SCDAP/RELAP5 Mod3.1 (Release D) developed by INEEL[6] which is well validated for thermohydraulics in RCS and relatively early phase of core degradation. The models of RELAP5 calculate the overall RCS thermal hydraulics, control system interactions, reactor kinetics, and the transport of noncondensable gases. The RELAP5 code is based on a non-homogeneous and non-equilibrium model for the two-phase systems, that is solved by a fast, partially implicit numerical scheme to permit economical calculation of system transient. The SCDAP code models the core behavior during a severe accident. The treatment of the core includes the fuel rod heatup, ballooning and rupture, FP release, rapid oxidation, zircaloy melting, UO_2 dissolution, ZrO_2 breach, flow and

freezing of the molten fuel and cladding, debris formation and behavior, control rod and shroud behavior.

4.2 Analytical Sequences

Four calculations with SCDAP/RELAP5 (S/R5) and two calculations with ART were performed in the present study. Analytical sequences and their assumptions are shown in **Table 4.1**. At first, two SCDAP/RELAP5 calculations (cases 1 and 2) were performed for Surry TMLB' sequences with and without secondary system depressurization to determine the thermohydraulic conditions for FP deposition calculation with ART. After that, two ART calculations (cases 3 and 4) were conducted by using the SCDAP/RELAP5 results. Finally, two SCDAP/RELAP5 calculations (cases 5 and 6) were performed with consideration of the decay heat from deposited FPs which were calculated by ART.

It was assumed that all the pump seals were kept intact during these sequences. In the case with secondary system depressurization, all the MSRVs were intentionally opened at 300 s after accident initiation. The present calculations were continued up to the onset of first boundary failure of RCS because the present calculation aimed mainly at the SG U-tube integrity. According to the INEEL's SCDAP/RELAP5 calculation with the same input deck, the timing of creep rupture failure of RPV lower head is 220 min (13,200 s) behind that of pressurizer surge line failure.

4.3 Input Data and Analytical Assumptions

4.3.1 Thermohydraulic Analyses (No Decay Heat)

The SCDAP/RELAP5 input data was prepared based on the original Surry input deck which includes some proprietary information and was used for analysis of TMLB' sequence at INEEL[9]. The Reactor Coolant System (RCS) and RPV (Reactor Pressure Vessel) nodalization for Surry analysis is shown in **Figs.4.2 and 4.3**, respectively. RPV was modeled with a downcomer, core bypass and five channels in the core and upper plenum. RCS was modeled as three coolant loops individually with more than 200 volumes and heat structures. The loop C has a pressurizer. The outer surface of the primary system is assumed to be adiabatic in this modeling.

During PWR severe accidents, the hot leg countercurrent natural circulation (CCNC) flow could occur as described in chapter 2. In order to simulate the CCNC flow, a special nodalization as shown in **Fig.4.4** was also prepared originally by INEEL based on the calculation with a three

dimensional fluid dynamic code, COMMIX for the Westinghouse one-seventh scale experiments on natural circulation. The hot leg was divided into upper and lower halves. The SG inlet plenum was divided into three volumes to allow for the plenum mixing of hot and cold flow streams. The SG U-tube was divided into two volumes to carry cold and hot flow streams. While this model is used, loop seal is made at the cross over leg and therefore most of steam flows backward at the SG outlet and goes back to the lower hot leg. It is noted that the RCS nodalization as shown in **Fig.4.2** was used up to the onset of core heat up and then the hot leg CCNC model was used.

In TMLB' sequence of Surry plant, the calculation with CCNC predicts about 2,000 s delay of fuel cladding failure compared with the calculation without CCNC because the hot-leg countercurrent flow enhances the heat transfer from the core to steam at an early stage of core heatup and as a result, the fuel cladding heatup can be delayed. On the other hand, use of CCNC model would result in higher temperature of hot-leg at a late phase of TMLB' sequence than that without CCNC model because the hot-leg countercurrent flow, on the contrary, could enhance the heat transfer from high temperature core to the hot leg structure by superheated steam flow[33].

4.3.2 FP Deposition Analysis

The boundary conditions for FP deposition analysis with ART code were determined as follows. The gas and wall temperatures at SG U-tube at the time of FP deposition initiation were defined based on the SCDAP/RELAP5 calculation without decay heat from deposited FP. The concentrations of CsI and CsOH in superheated steam at hot leg were taken from a similar MELCOR calculation for TMLB' sequence of Surry plant[18]. The concentrations are mostly equal to the averaged value at the hot leg inlet during the time of temperature escalation due to Zr-water reaction. That is, the gas concentrations of CsI and CsOH at hot leg are 0.006 and 0.040 kg/m^3, respectively. The ART input data for SG U-tube integrity analyses for cases 3 and 4 are shown in **Appendix 1 and 2**, respectively.

In the SCDAP/RELAP5 calculation for definition of ART boundary conditions, 3 m long volume was used for SG U-tube while 30 cm long volume was used in the ART calculation to simulate precisely the local FP deposition distribution and decay power at the SG U-tube inlet. However, when the SCDAP/RELAP5 calculation is performed considering the decay heat calculated by ART, the length of volume in SCDAP/RELAP5 was not shortened as in the ART calculation because a smaller time step, that is, much CPU time would be needed from the Courant constraint if the shortened volume is used. Taking into account the purpose of present study and the

local creep rupture occurrence, use of long volume for SG U-tube in the SCDAP/RELAP5 calculation is not considered to affect so much the results.

The decay heat from deposited FPs are proportional to the deposition mass which depends mostly on the FP concentration in gas phase and the temperature difference between gas and wall because the principal FP aerosol deposition mechanism is thermophoresis. Therefore, in order to predict precisely the FP deposition mass, thermohydraulic and FP behavior calculations have to be coupled with each other. However, it is not easy to couple independent SCDAP/RELAP5 and ART calculations. Therefore, in the present calculation, the decay power from deposited FP was assumed to be constant for simplification although the FP deposition mass, in reality, increases linearly as time goes on. The constant decay power was defined from the calculated deposition mass at 2,000 s after deposition initiation. The duration of 2,000 s is also just one of assumptions. It was also assumed for simplification that FP deposition begins to occur when the fuel temperature reaches 1,500 K because most of FP release would begin above the fuel temperature of 1,500 K.

4.3.3 Thermohydraulic and Structural Response Analyses

The decay heat from deposited FP calculated by ART was then given to the heat structures of SG U-tube inlet in the SCDAP/RELAP5 calculation. Finally, thermohydraulic and structural response calculations with consideration of decay heat from deposited FP were performed with SCDAP/RELAP5 in the case with and without the secondary system depressurization.

The cladding oxidation models used in the present calculation were the Cathcart-Pawel and the Urbanic-Heidrick models. The creep rupture calculation was performed for hot leg, surge line, SG U-tube and RPV bottom head by using the Larson-Miller theory[19]. The break area of creep rupture was assumed to be 0.19034 ft^2 or 0.01769 m^2 which is the same size as in the USNRC's calculation[7].

4.4 Analytical Results

4.4.1 Thermohydraulic Analyses with SCDAP/RELAP5 (No Decay Heat)

As a first step, two calculations (cases 1 and 2) with SCDAP/RELAP5 were performed to determine the boundary conditions for FP deposition calculations at SG U-tube during TMLB' sequence with and without MSRV bleed operation.

The steam and wall temperatures at SG U-tube calculated from the SCDAP/RELAP5 calculations are shown in **Fig. 4.5**. It is noted that the axial temperature distribution of wall and gas at SG U-tube inlet were defined by linearly interpolating the calculated temperatures between steam generator inlet plenum and first volume of SG U-tube. These temperature distribution correspond to the timing of fuel temperature equal to 1500 K in each case. It is noted that the decay heat from deposited FP was not taken into account in these calculations. The calculated steam velocity and Reynolds number in SG U-tube were approximately 0.5 m/s and 12,000, respectively. These boundary conditions were given to the FP deposition calculation with ART as the input.

There could be a discussion in determining the steam temperature at SG U-tube inlet because steam comes into the SG U-tube inlet (volume 408-01) from the inlet plenum volumes with and without mixing (volumes 406 and 405), respectively. The temperatures of steam and wall at SG inlet plenum and first SG U-tube volumes with and without secondary depressurization at the time of the core temperature equal to 1500 K (Cases 1 and 2) are shown in **Table 4.2**.

It is considered that some uncertainties were included in these calculations and modeling because the core temperature of Westinghouse experiment cannot be raised up to, for example 1273 K due to the facility limitations and therefore the degree of superheating at hot leg may not have been sufficient in the experiment. Moreover, SF_6 was used instead of steam as coolant although the thermal properties of SF_6 at relatively low temperature are similar to those of steam at high temperature. Therefore, it is slightly questionable that the present hot leg countercurrent flow model can be applied to the case such as severe conditions just before surge line or hot leg creep failure.

Moreover, it is slightly difficult to consider that all the steam from the volumes 406 and 405 can be mixed uniformly just before the SG U-tube inlet. From these reasons, we thought that the contribution of steam which passes through the SG inlet plenum cannot be ignored and the present study used unmixed vapor temperature at SG U-tube inlet, which may result in larger deposition mass due to thermophoresis, rather than mixed temperature in the calculation.

In the case without MSRV bleed operation, there is a large difference in temperature at SG U-tube inlet between steam and U-tube wall. Therefore, it is expected that the FP deposition mass increases due to thermophoresis or condensation at SG U-tube inlet. On the other hand, in the case with MSRV bleed operation, the temperature of SG U-tube wall is slightly higher than the case without MSRV bleed operation because the heat removal efficiency of secondary side is smaller due to secondary system depressurization. It can be pointed out that the temperature difference at SG

U-tube inlet is slightly larger than the case without MSRV bleed operation.

4.4.2 FP Deposition Analysis with ART

The averaged FP deposition velocity in the case with MSRV bleed operation is shown in **Fig. 4.6**. At SG U-tube inlet, the dominant deposition mechanism for aerosol is thermophoresis which depends on thermal gradient in gas phase. For the U-tube elevation above 1.0 m, deposition due to turbulent flow becomes dominant. Deposition velocity by Brownian diffusion is small along with the U-tube axis and can be ignored.

The gravitational settling was taken into account in the present calculation. However, the deposition mass due to gravitational settling was not so important at SG U-tubes from a view point of FP decay heating and therefore the FP deposition calculation was performed only for upward vertical U-tube up to 6 m high from the SG U-tube inlet and not for horizontal part of U-tube bend. Accordingly, the deposition velocity due to gravitational settling was not predicted in **Fig. 4.6** because of no deposition area at vertical pipe.

The deposited mass distribution along with the SG U-tube axis in the cases with and without MSRV bleed operation is shown in **Fig. 4.7**. In the case with MSRV bleed, large amount of CsOH and CsI were deposited at the SG U-tube inlet due to thermophoresis. The deposited mass of CsOH became larger by about one order of magnitude than that of CsI in proportion to concentrations of the two species. The decay heat from deposited FPs was evaluated at the SG U-tube inlet where the deposition mass was the largest. In the case without MSRV bleed, overall tendencies are almost the same as the case with MSRV bleed. However, calculated deposited mass at the U-tube inlet was slightly smaller than the case with MSRV bleed. This is because temperature difference at the SG U-tube inlet between steam and wall was slightly smaller than that in the case with MSRV bleed operation.

The deposited mass at SG U-tube inlet after the fuel temperature arrival at 1500 K in the case with MSRV bleed operation is shown in **Fig. 4.8**. It can be seen that both the deposited masses of CsOH and CsI increase linearly as a function of time. At 2,000 s after deposition initiation, the deposited masses of CsOH and CsI reached about 148 and 16 g/m^2, respectively.

As a second step, the decay heat from cesium and iodine was evaluated based on the decay heat table in the ART code. The table was prepared for unit nuclear power as a function of burnup

and time after scram. The decay power from iodine is larger by about one order of magnitude than that from cesium. The calculated total decay power from FP deposition at SG U-tube inlet is shown in **Fig. 4.9**. The decay power in the case with MSRV bleed operation became larger than that without MSRV bleed operation in proportion to the deposition mass of each case. At 2,000 s, the decay power in the case with and without MSRV bleed operation reached about 3,000 and 2,000 W/m^2, respectively.

4.4.3 Thermohydraulic and Structural Response Analyses with SCDAP/RELAP5

The primary system pressures during TMLB' sequence with and without MSRV bleed operation are shown in **Fig. 4.10**. In the case without MSRV bleed operation, the pressure temporarily decreased just after the accident initiation because fluid temperature at hot leg decreased due to scram. As soon as the pumps are tripped off, the pressure began to recover. However, while the SGs were effective as heat sink, the pressure was kept below normal operating level. When the SGs dryout occurred, the pressure rose to the PORVs' set point. The pressure oscillation continued due to opening & closing of PORVs. A creep rupture occurred at the pressurizer surge line at 15,300 s.

In the case with MSRV bleed operation, the pressure began to decrease after MSRVs opening at 300 s due to heat removal by flushing in secondary system. At about 2,000 s, the minimum pressure of 7.9 MPa was achieved. After that, the pressure began to increase due to dryout of secondary system and reached the PORVs set point at 4,300 s. The pressure oscillation continued until a creep rupture of the surge line at 13,500 s.

The secondary system pressures in the cases with and without MSRV bleed operation are shown in **Fig. 4.11**. In the case without MSRV bleed operation, the pressure was kept at the MSRVs set point. After the SGs dryout, the cycle of MSRVs' opening & closing became long due to decrease in steam generation at secondary side. In the case with MSRV bleed operation, the pressure began to decrease after MSRVs opening at 300 s and reached the atmospheric pressure at 2,200 s.

The maximum fuel temperature in the core in the case with MSRV bleed operation is shown in **Fig. 4.12**. The temperature began to increase at 8,300 s and reached 1,500 K at 12,400 s. In the present calculation, it was assumed that serious CsI and CsOH releases from fuel and their deposition onto RCS begin at the fuel temperature above 1,500 K for simplification.

The gas velocity at lower hot leg in the case with MSRV bleed operation is shown in **Fig. 4.13**. This curve corresponds to the gas velocity at junction No.431 between the lower hot leg and RPV. It is noted that the hot leg nodalization was switched to the CCNC model at 8,300 s. The rapid backward flow was calculated periodically because of the opening & closing of PORVs. Calculated countercurrent flow velocity at lower hot leg is about 0.3 m/s.

The temperatures of pressurizer surge line, hot leg and SG U-tube in the case with MSRV bleed operation are shown in **Fig. 4.14**. It is noted that the decay heat from deposited FPs was not considered in this case. The temperatures began to increase after 8,300 s. The surge line temperature slightly oscillated at the time of PORVs opening & closing and began to increase at 10,500 s because of the heat transfer from increased steam temperature inside hot leg which was caused by increase of core temperature by cladding oxidation and decay heat from fuel. The earliest creep rupture occurred at surge line at 13,500 s because the surge line temperature increased the fastest due to superheated steam flow toward PORVs and smaller thermal mass than that of hot leg. The surge line temperature at the creep rupture was 1,100 K.

The heat generated by cladding oxidation was of course taken into account in our calculation. The cladding oxidation models used in our calculation were Cathcart-Pawel and Urbanic-Heidrick models depending on the cladding temperature. As shown in my slide on page 20, the surge line temperature began to increase at 10,500 s because of the heat transfer from increased steam temperature inside hot leg which was caused by increase of core temperature by cladding oxidation and decay heat from fuel.

The temperatures of SG U-tube and surge line considering decay heat in the case without MSRV bleed operation are shown in **Fig. 4.15**. The temperature of SG U-tube abruptly increased at 13,950 s because the fuel temperature reached 1,500 K at that time and FP release & deposition began to occur based on the assumptions described in II. 2. (1). The calculations showed that the earliest creep rupture would occur at surge line if the decay heat from FPs deposited onto SG U-tube is smaller than 11,000 W/m^2. However, the earliest creep rupture location would be changed from surge line to SG U-tube if the decay heat at SG U-tube is larger than 12,000 W/m^2. According to the ART calculation, the decay heat in this case is about 2,000 W/m^2 and therefore there is a certain room for SG U-tube integrity.

The temperatures of SG U-tube and surge line considering decay heat in the case with MSRV bleed operation are shown in **Fig. 4.16**. The temperature of SG U-tube abruptly increased at 12,400 s due to the same reasons described above. The calculations showed that the earliest creep rupture would occur at surge line if the decay heat at SG U-tube is equal to or smaller than 3,000 W/m^2. However, the earliest creep rupture location would be changed from surge line to SG U-tube if the decay heat is larger than 4,000 W/m^2. It is noted that the creep rupture temperature of SG U-tube in this case becomes lower by 80 K than the previous figure due to larger pressure difference between primary and secondary systems. According to the ART calculation, the decay heat in the case with MSRV bleed operation is about 3,000 W/m^2. Therefore, it can be said that there is very little room for SG U-tube integrity during secondary system depressurization. Taking into account some uncertainties in the present analyses, the occurrence of SGTR cannot be ignored when the secondary system is depressurized.

Table 4.1 Analytical sequences and assumptions

Reference plant; Surry	Sequence; TMLB'					
	Case 1	Case 2	Case 3	Case 4	Case 5	Case 6
Computer code	S/R5	S/R5	ART	ART	S/R5	S/R5
MSRV bleed at 300 s	No	Yes	---	---	No	Yes
T-H boundary conditions	---	---	Case 1	Case 2	---	---
Decay heat from deposited FP	No	No	---	---	Yes (Case 3)	Yes (Case 4)

Assumptions
- No pump seal failure
- After onset of core heat up, consideration of hot leg countercurrent natural circulation flow
- FP deposition initiation at the time of fuel temperature equal to 1500K
- Constant decay power defined from deposited CsI and CsOH masses at 2000 s after deposition initiation
- Creep rupture calculation by using Larson-Miller theory
- Break area equal to 0.19034ft^2 or 0.01769m^2

Table 4.2 Temperatures of steam, wall at SG inlet plenum and first SG U-tube volumes at time of core temperature equal to 1500 K

		Without secondary depressurization	Secondary depressurization
Time after accident initiation		(Case 1) 13,950 s	(Case 2) 12,400 s
SG plenum without mixing (volume 405)	steam	962 K	998 K
	wall	738 K	751 K
SG plenum with mixing (volume 406)	steam	761 K	786 K
	wall	669 K	678 K
SG U-tube first (volume 408-1)	steam	737 K	784 K
	wall	720 K	781 K

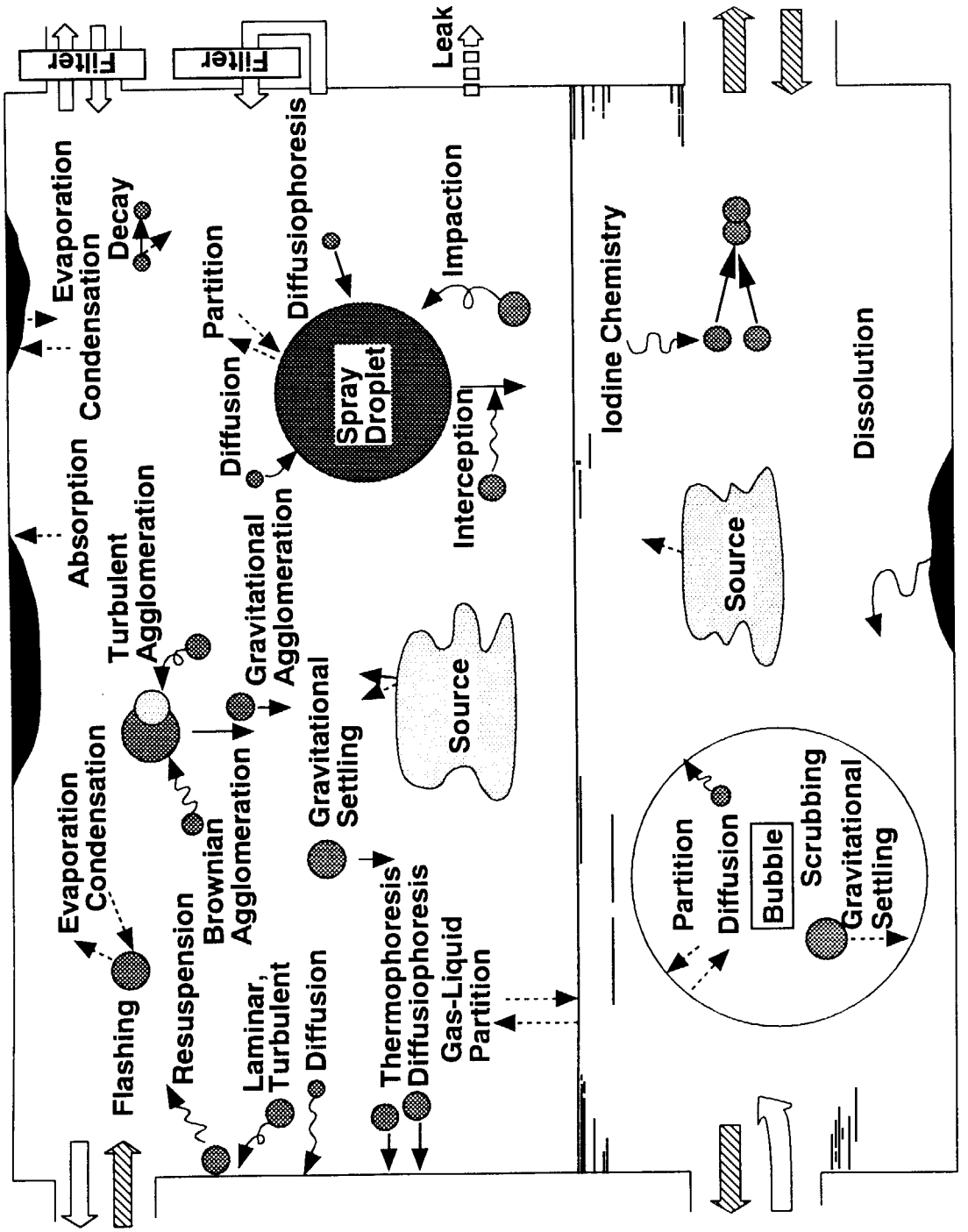

Fig.4.1 Radionuclides transport and deposition in ART Mod 2

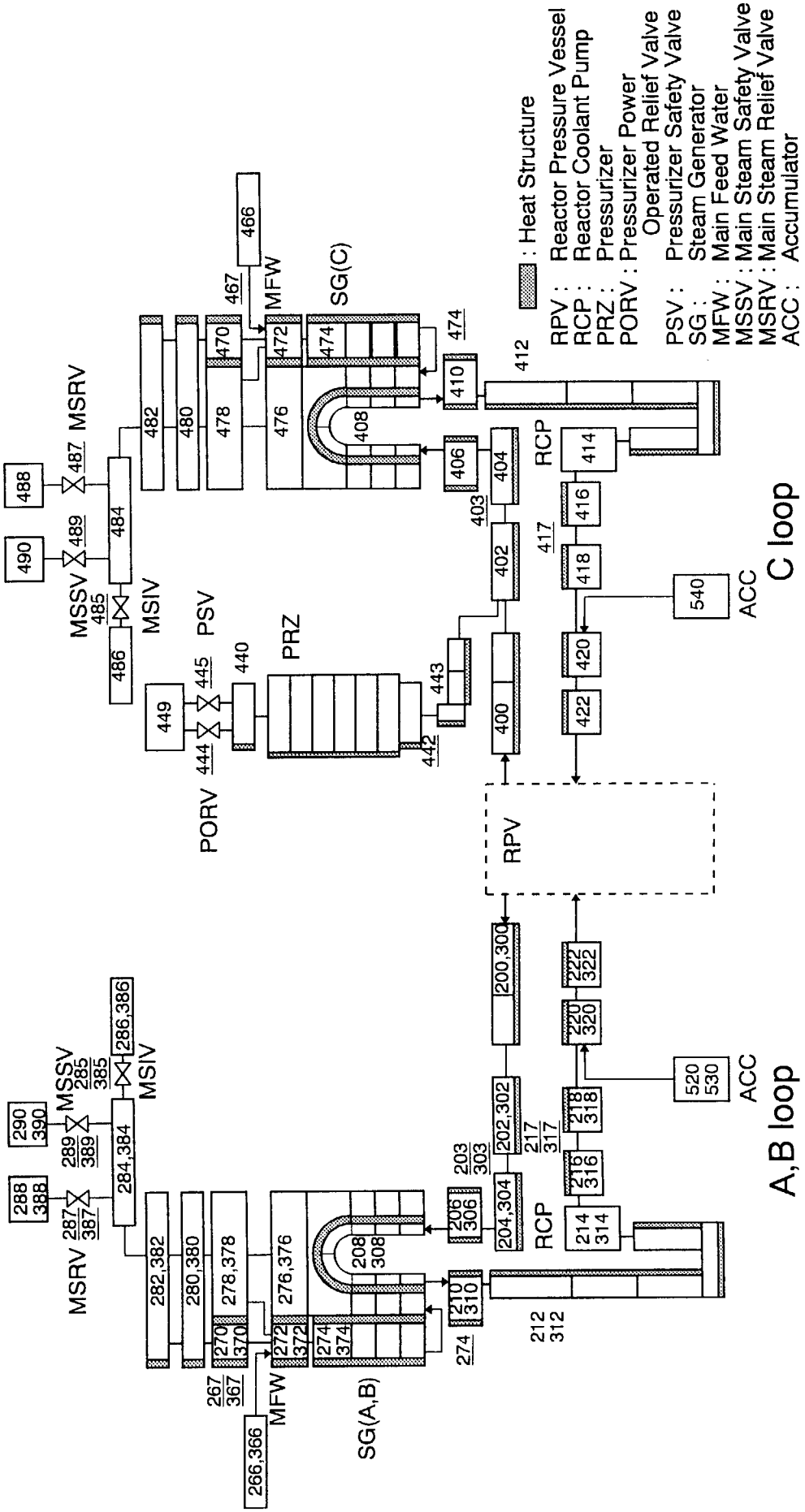

Fig.4.2 SCDAP/RELAP5 nodalization for Surry RCS

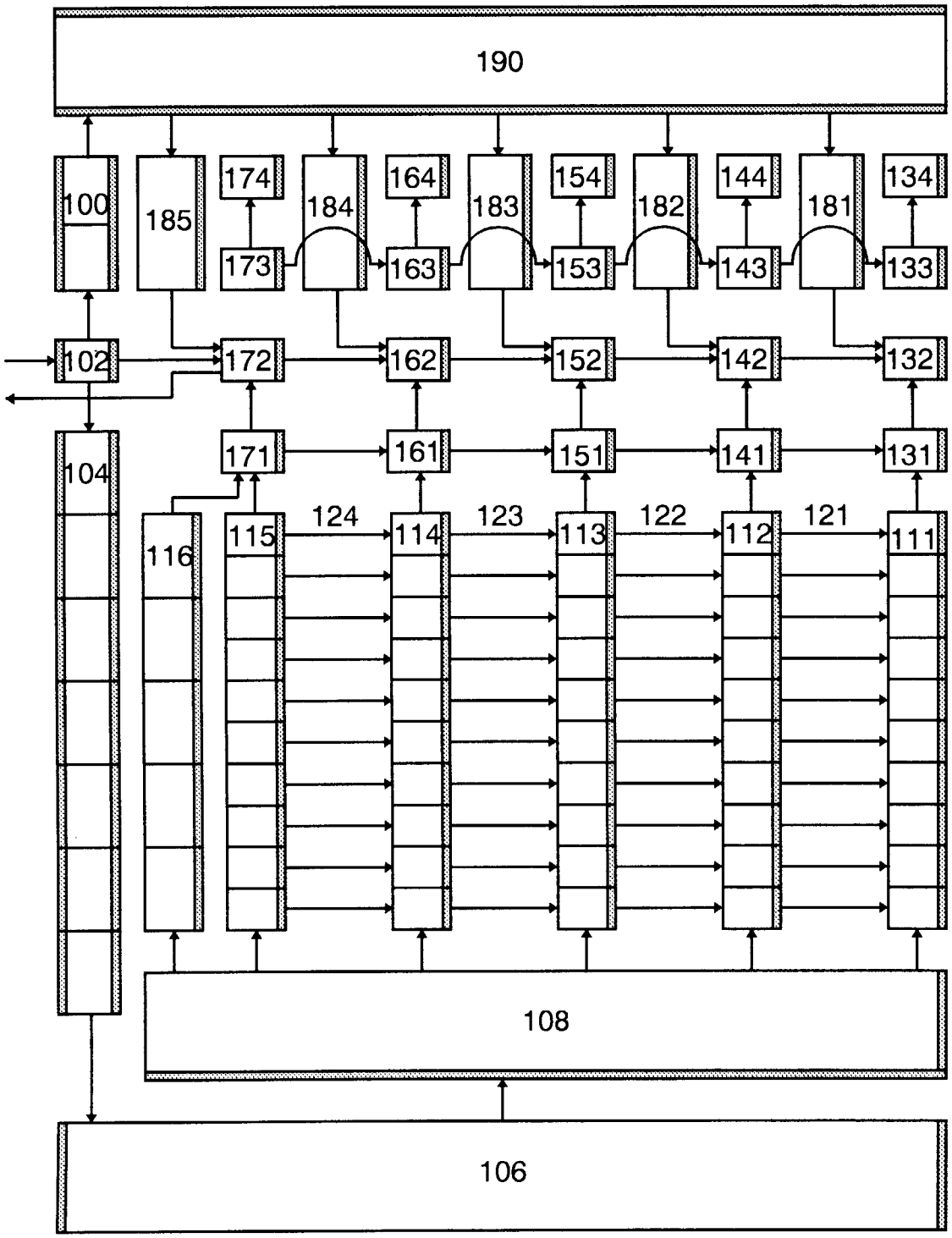

Fig.4.3 Nodalization for Surry RPV

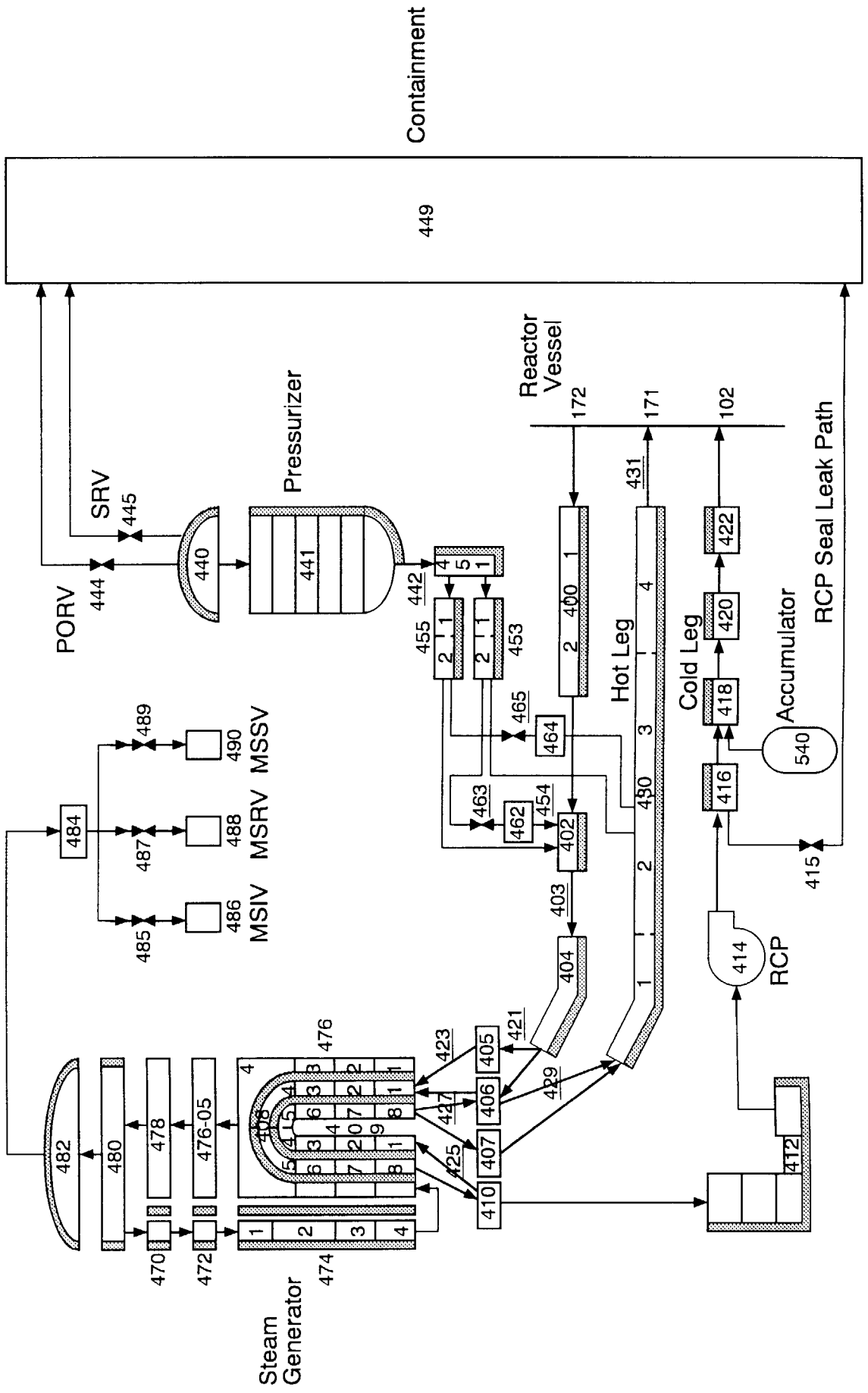

Fig.4.4 Countercurrent natural circulation model for Surry hot leg

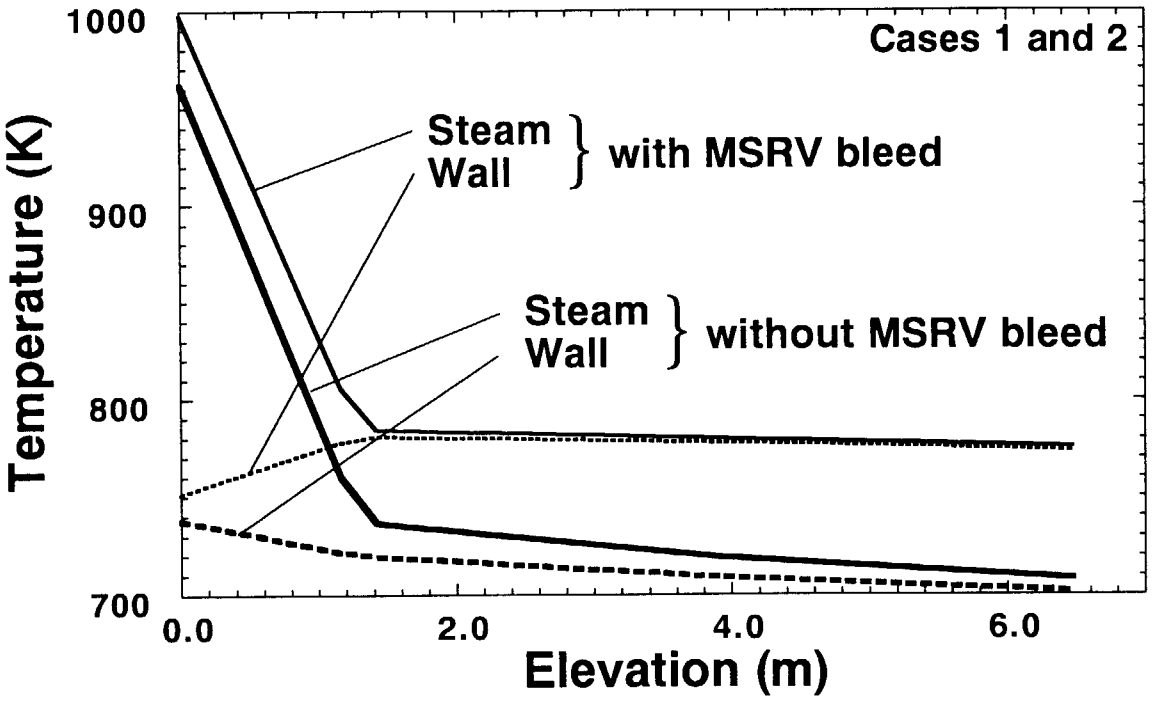

Fig.4.5 Temperature distribution in SG U-Tube without decay heat

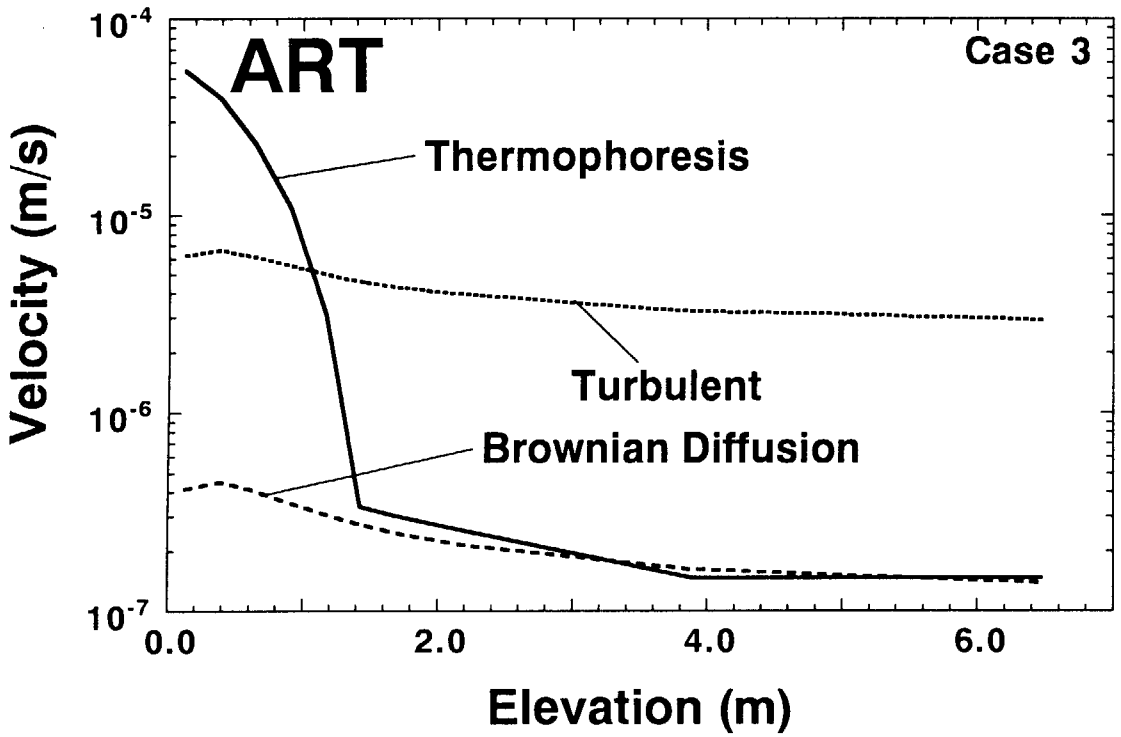

Fig.4.6 Averaged FP deposition velocity at SG U-tube (without MSRV bleed)

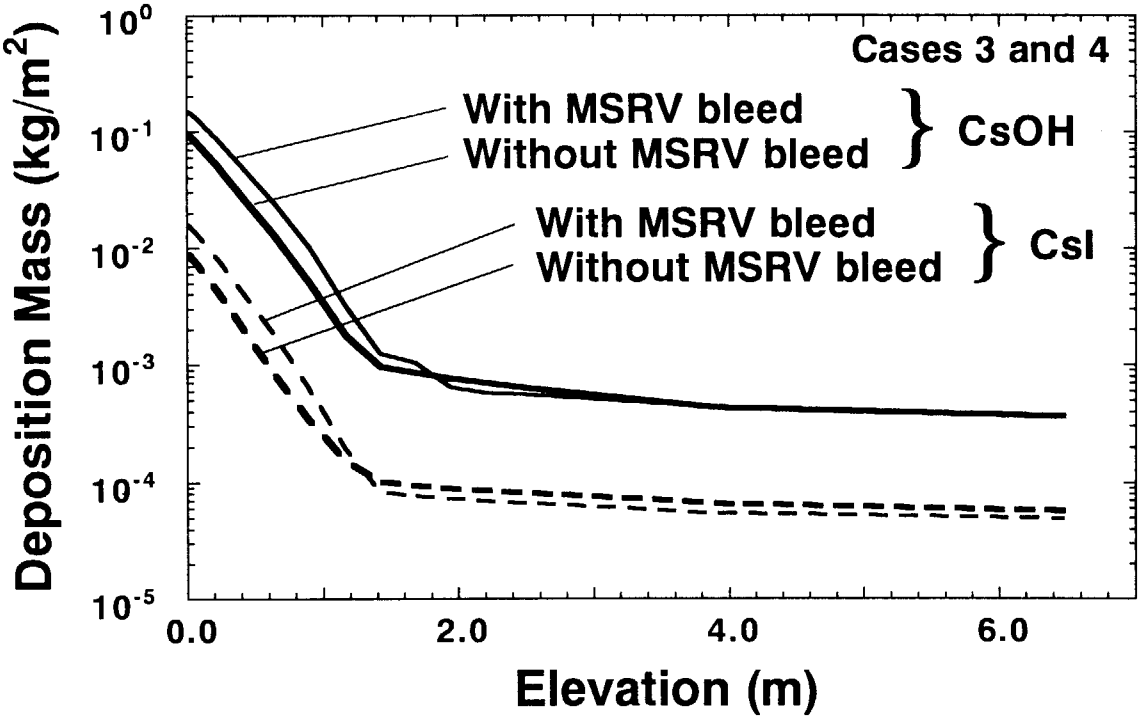

Fig.4.7 Deposition mass distribution at SG U-tube(with & without MSRV bleed)

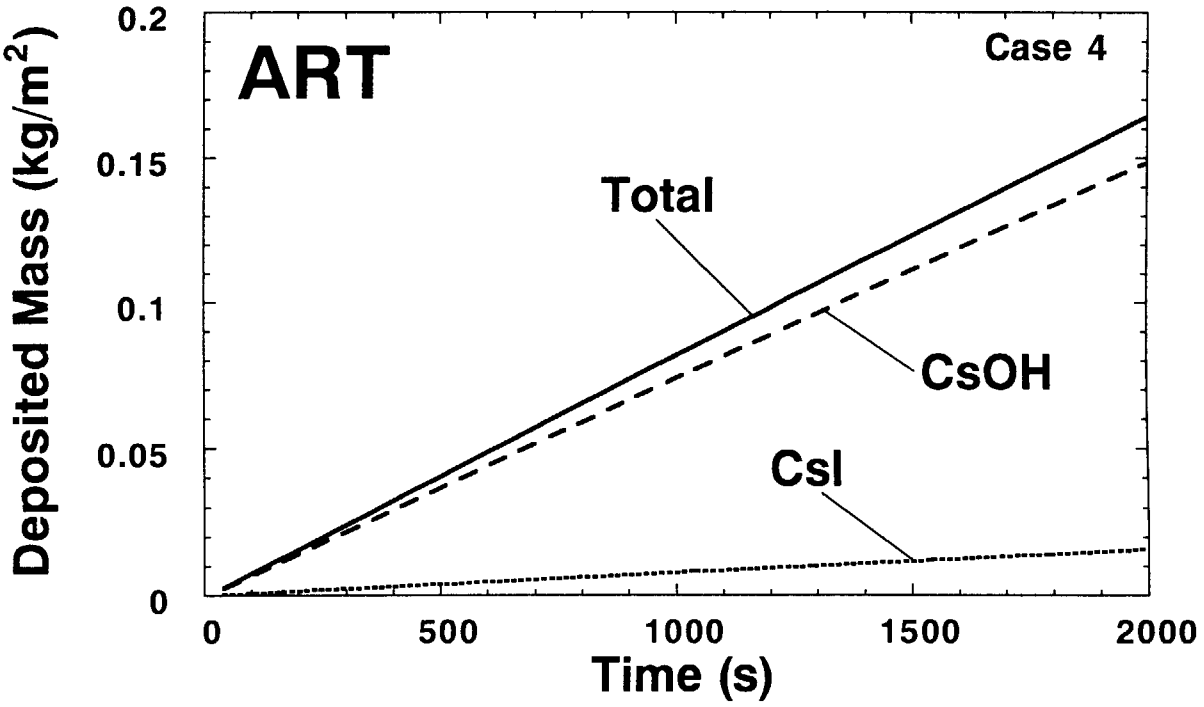

Fig.4.8 Deposited mass at SG U-tube inlet (with MSRV bleed)

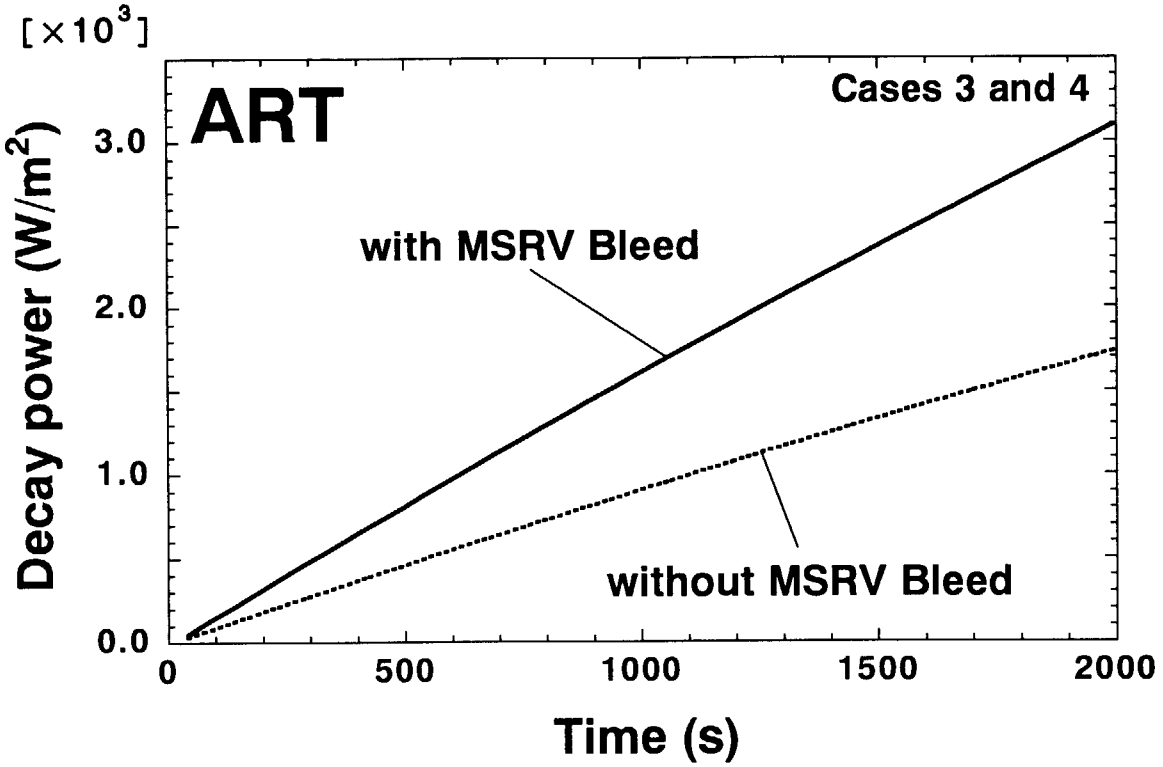

Fig.4.9 Decay power at SG U-tube inlet

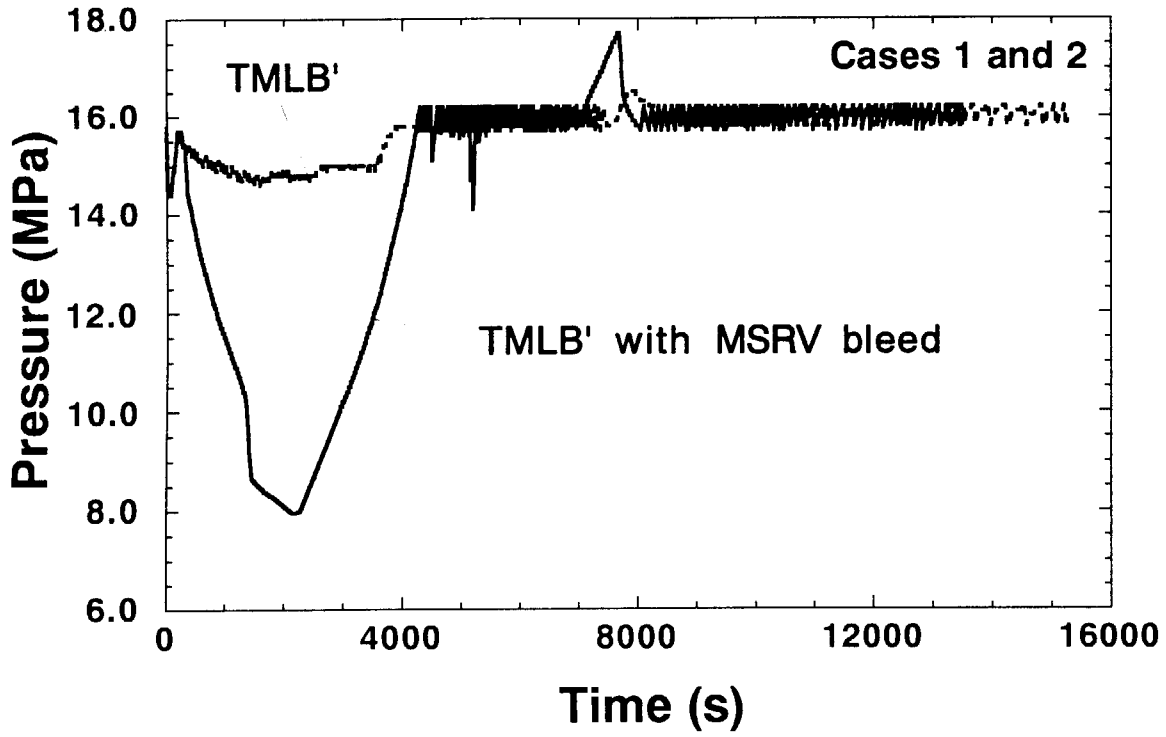

Fig.4.10 Primary system pressure

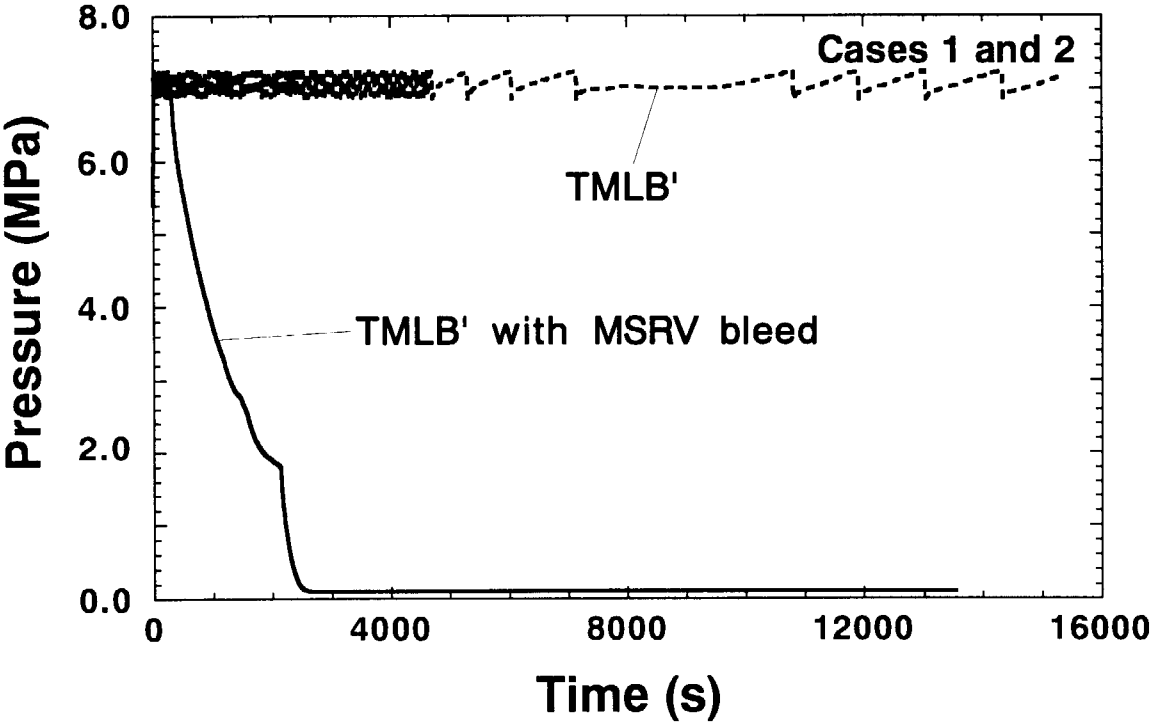

Fig.4.11 Secondary system pressure

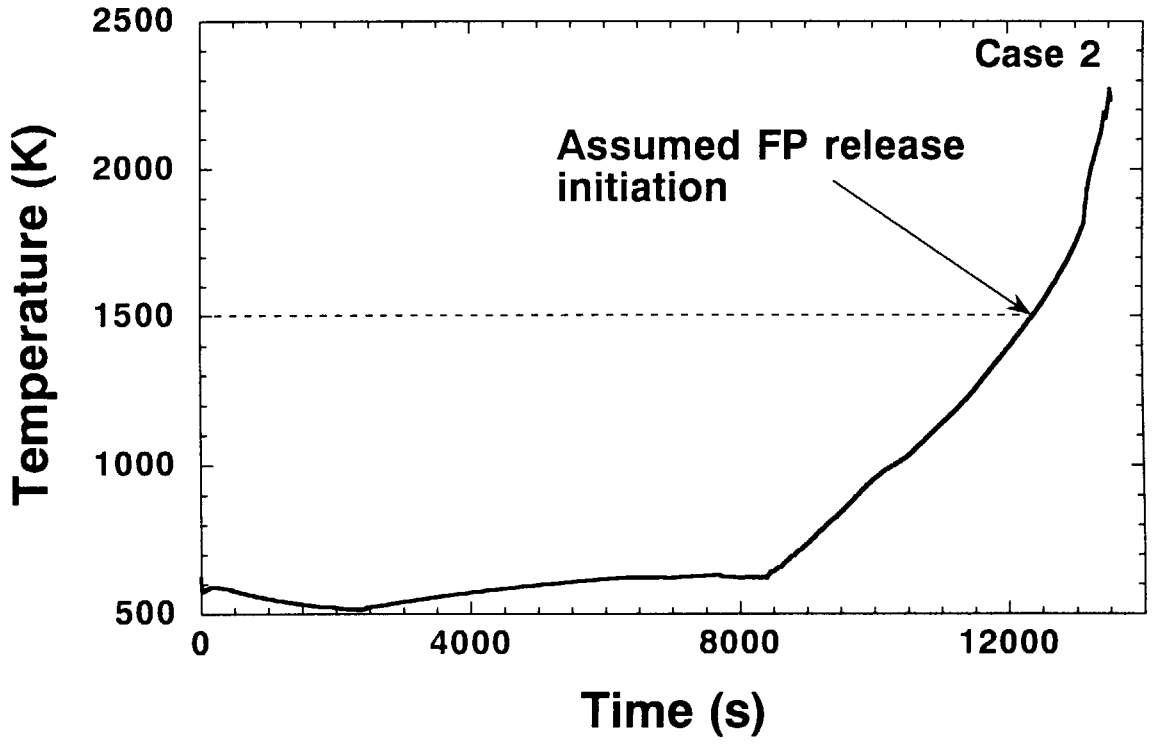

Fig.4.12 Maximum fuel temperature (with MSRV bleed)

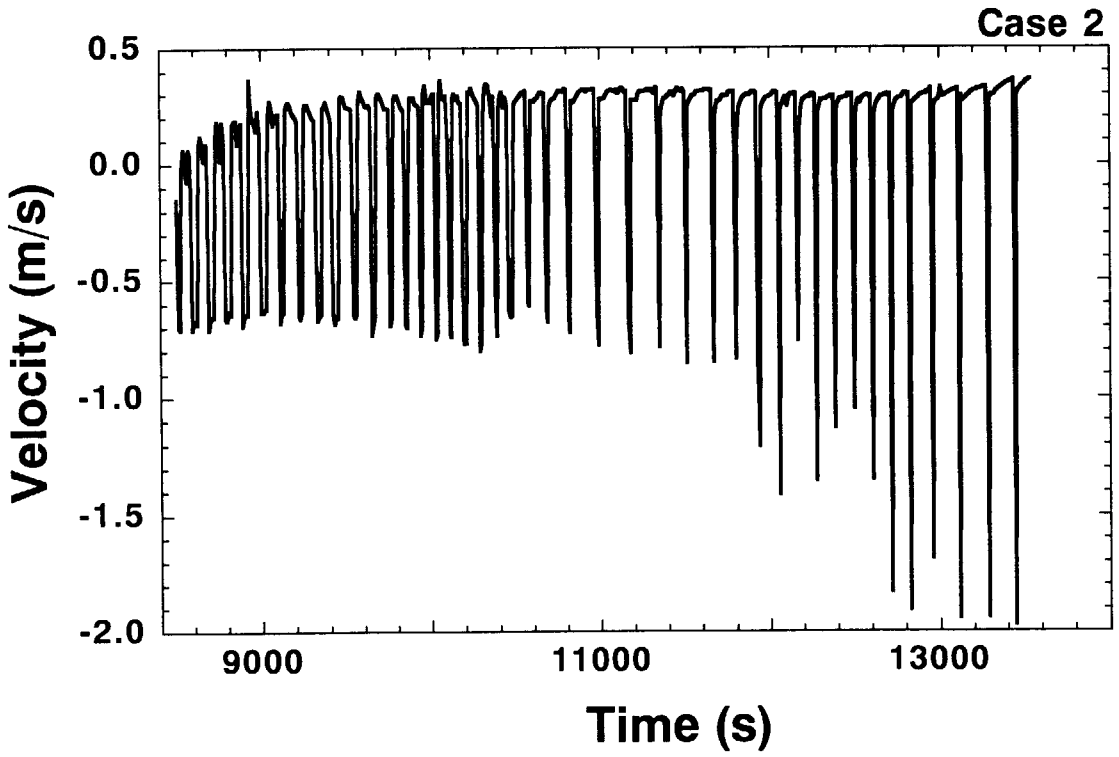

Fig.4.13 Gas velocity at lower hot leg (with MSRV bleed)

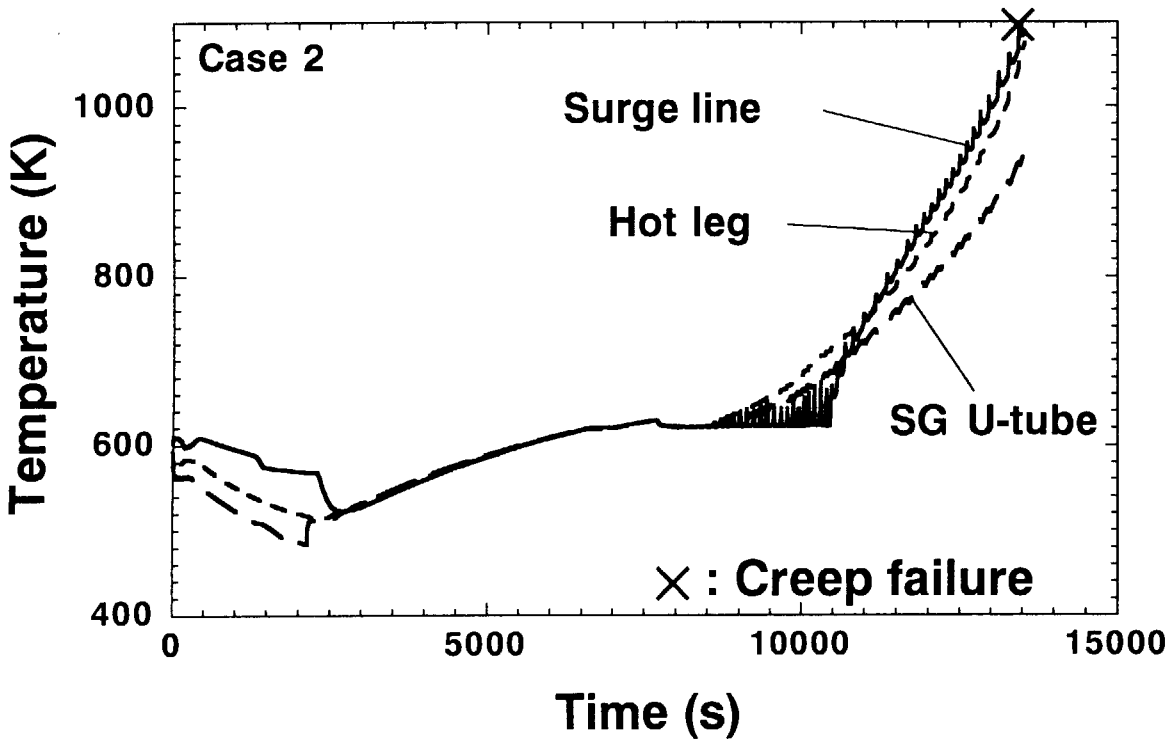

Fig.4.14 Structural temperatures (with MSRV bleed)

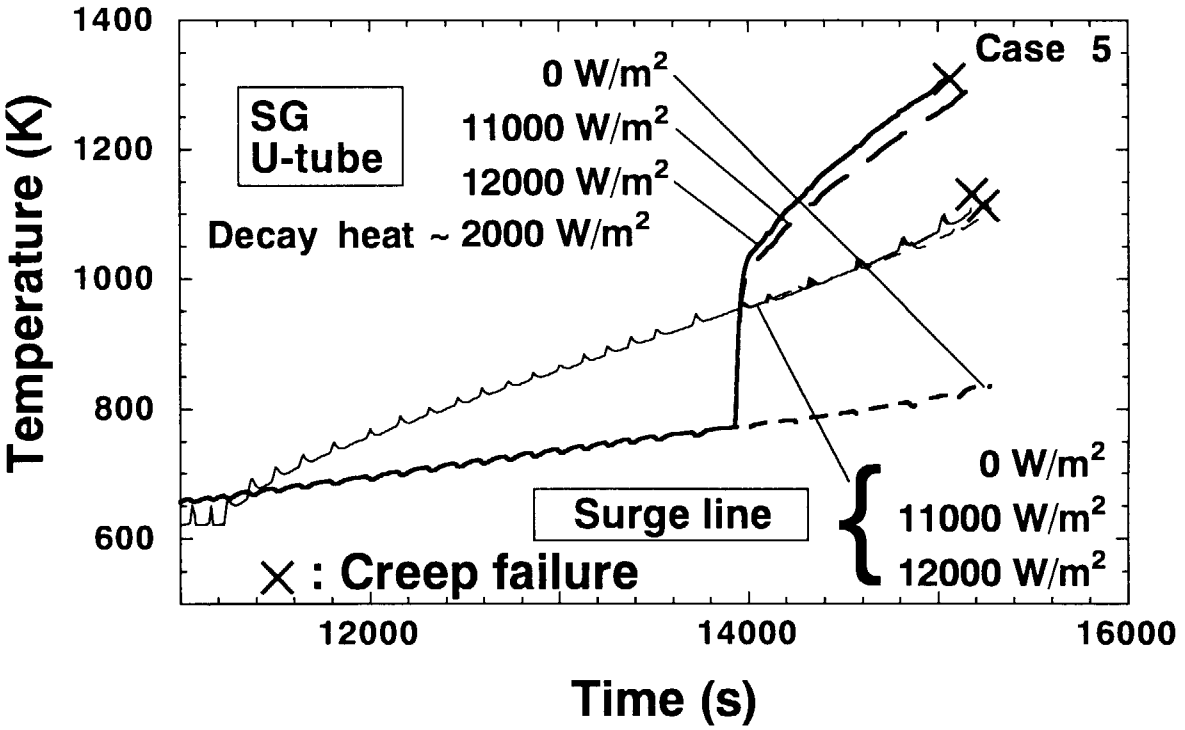

Fig.4.15 Temperature of SG U-tube and surge line (without MSRV bleed)

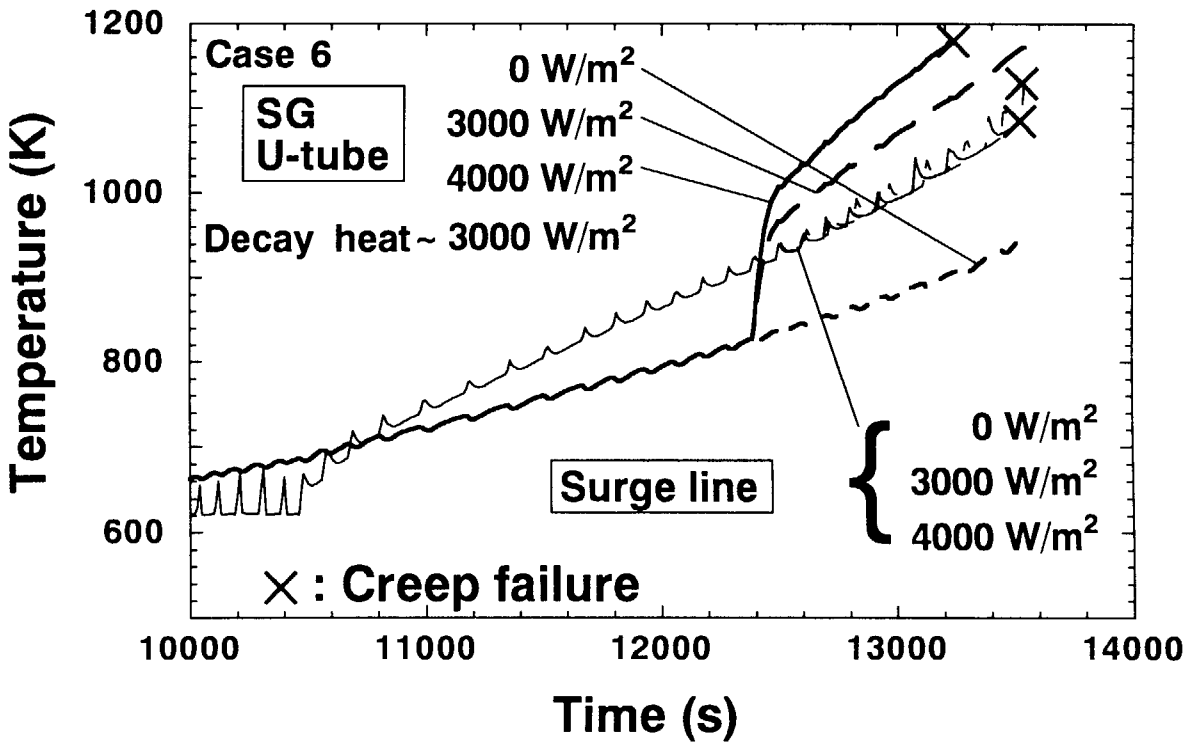

Fig.4.16 Temperature of SG U-tube and surge line (with MSRV bleed)

5. DISCUSSIONS

5.1 Comparison with USNRC's Calculation

The present SCDAP/RELAP5 calculations without decay heat from deposited FP (cases 1 and 2) were in reasonable agreement with the USNRC's calculations[7]. On the other hand, in the case with the FP decay heat, the present calculation (case 6) showed that the decay heat from deposited FP plays an important role on the RCS structural response analyses during TMLB' sequence with the secondary system depressurization.

However, in the USNRC's SCDAP/RELAP5 calculation, the effect of decay heat from deposited FP was not taken into account in the evaluation of the SG U-tube integrity during TMLB' sequence with the secondary system depressurization. This is because USNRC's separate study with the VICTORIA code[20] showed that the FP transport and deposition in the RCS have a negligible effect on the SG U-tube integrity since the FP release is relatively small at the time of RCS failure and the predicted mass of FP deposition can be ignored. The calculated dominant mechanisms for FP deposition at SG U-tube was settling inside of the SG U-tubes onto the upward facing surfaces in the bends of the U-tubes[7].

However, it should be pointed out that "thermophoresis" which is highly probable at thermal gradient tubes such as SG U-tube was not predicted as one of dominant mechanisms in the USNRC's VICTORIA calculation. This is because the length of first node at SG U-tube inlet used in the USNRC's FP deposition calculation was about 2.6 m which is the same as the length in SCDAP/RELAP5 calculation (see **Fig. 4. 4**). Therefore, in spite of high temperature of steam at the SG U-tube inlet, a representative (averaged) steam temperature at the first node was decreased and mostly equal to the SG U-tube wall temperature which mostly agrees with the secondary system temperature. Moreover, completely mixed steam temperature from volumes 405 and 406 was used in the USNRC's calculation. As a result, a temperature difference of about 15 K in this region, which results in minimal deposition by thermophoresis in the USNRC's calculation.

In the present study with JAERI's FP deposition analysis code, ART, the length of first node at SG U-tube was shortened up to about 30 cm and careful attentions were paid to consideration of high temperature of superheated steam at the SG U-tube inlet in the FP deposition analysis. Moreover, unmixed steam temperature from volume 405 was used as the steam temperature at SG U-tube inlet. This assumption may overestimate the temperature difference in steam and wall at SG U-tube inlet and would result in large deposition mass by thermophoresis. However, this slightly

conservative assumption was used in the present study because it is unlikely to consider that instantaneous steam mixture from 405 and 406 volumes is established at the SG U-tube inlet. Consequently, ART calculation showed relatively large amount of FP deposition in that region. Summary of comparison between USNRC's VICTORIA and JAERI's ART calculations is shown in **Table 5.1**.

5.2 Feedback of Thermohydraulics Change on FP Deposition Calculation at Every Time Step

The detailed change of thermohydraulic conditions such as increase in pipe wall temperature due to decay heat from deposited FP was not reflected at every or short time step on the FP deposition calculation with ART code. Instead, the constant thermohydraulic conditions at RCS such as gas velocity, temperature, and wall temperature at the time of fuel temperature equal to 1500 K were always used for simplification in the present calculation. In order to consider the detailed change of thermohydraulic conditions due to FP decay heat, a kind of feedback calculation between SCDAP/RELAP5 and ART has to be done many times. It is noted that the handling of feedback calculation is not easy and the calculation requires huge computation time.

5.3 Revaporization of Deposited or Condensed FP

If the pipe wall temperature exceeds the melting temperature of FP, the deposited or condensed FP onto the pipe could be revaporized excepting the chemisorbed deposition of gaseous FP. For example, in the case of CsI, CsOH, Te, Sr and Ba, those melting temperatures are 894, 588, 723, 1070 and 1263 K, respectively. Therefore, the present FP deposition calculation in which only the CsI and CsOH were assumed as species of FP and the constant thermohydraulics conditions at RCS were used may underestimate the revaporization of deposited or condensed FP and as a result, overestimate the mass of FP deposition or condensation. However, the revaporization of some radionuclides such as Te and Ba would be limited because they have relatively high melting temperature. It is noted that they have high release rate depending on the atmospheric conditions and also have high decay heat at about 10,000 s after accident initiation.

5.4 Effect of Decay Heat at Hot Leg and Surge Line

Relatively large amount of FPs could be deposited at hot leg mainly due to condensation of FP gas and there would be no large difference in deposited mass between hot leg and SG U-tube.

However, the thermal mass of hot leg is fairly larger than that of SG U-tube and therefore the hot leg temperature would increase by only a few K due to decay heat although the SG U-tube temperature increases by a few hundred K. In the case of pressurizer surge line, the gas flow velocity at the time of PORV opening is about 30 m/s and some of deposited FPs would come back to gas flow due to resuspension. Moreover, the thermal mass of surge line is slightly smaller than that of hot leg but it is still fairly larger than that of SG U-tube. Therefore, the decay power from deposited FP can be ignored at surge line.

5.5 Enhancement of FP Deposition onto Upward Pipe

A relatively small-scale aerosol deposition experiment (called WAVE; Wide range Aerosol model VErification) using a 90 degree bend quartz glass pipe with a short straight part on the downstream side have been performed at JAERI to investigate the effect of flow direction on the cesium iodide (CsI) aerosol behavior[21]. Three experiments in which the downstream flow after the bend were horizontal, upward and downward, respectively, showed 10 times larger CsI deposition mass in the vertical section of pipe with upward bend than those with horizontal and downward bends. It was found out by observation from the outside of quartz glass that only the flow regime in the vertical section of pipe with upward bend is changed from laminar to turbulent flow because of the secondary flow in the vertical pipe which flows opposite to the main forced convection. However, the Reynold's number calculated from the main forced convection was equal to about 300. It is noted that a laminar flow regime was maintained in the horizontal and downward pipes while the same thermohydraulic conditions as the upward vertical pipe were used.

Analyses of the experiments have been conducted with a three-dimensional fluiddynamic and a FP aerosol behavior analysis codes. The calculations showed that the principal CsI deposition mechanism at the upward vertical pipe is thermophoresis which is a function of thermal boundary layer thickness, δt calculated from the Nusselt number and representative length, D as shown in Eq.(3.1). In the calculation with the Nusselt number for laminar flow, the deposited mass of CsI was underestimated by about one order of magnitude while a sensitivity calculation was in reasonable agreement with the measurement in the case with the Nusselt number for turbulent flow.

In the present study with ART code, the Nusselt number for turbulent flow was used for calculating the thermophoretic FP deposition onto the upward vertical pipe such as SG U-tube inlet since the Reynold's number of main forced convection was 12,000. However, the Nusselt number could become larger than the present value if the secondary flow in the vertical pipe which flows

opposite to the main forced convection is taken into account. The larger Nusselt number results in smaller thermal boundary layer thickness. Consequently, the deposition mass at SG U-tube inlet could become larger than the present calculation.

5.6 Other Phenomena which Threaten the Integrity of SG U-Tube

The heat transfer from steam generator U-tube to secondary side could be smaller than the theoretical value as used in the present calculation because the sludge included in the secondary coolant would deposit onto outer surface of steam generator U-tube and could decrease the heat transfer rate between SG U-tube and secondary side[7]. This could become thermal insulation and accelerates the SG U-tube temperature increase.

As discussed above, there are associated uncertainties in the evaluation of SG U-tube integrity during TMLB' sequence with the secondary system depressurization. Therefore, it is difficult to conclude that the potential for SGTR can be ignored as in the USNRC's evaluation. However, it should be also pointed out that present study indicated unlikelihood of SGTR in the case of secondary system feed operation before the core temperature increase. These should be also considered in the evaluation of merits and demerits of accident management measures relating to the secondary system depressurization.

Table 5.1 Comparison between USNRC's VICTORIA and JAERI's ART calculations

	VICTORIA	ART
- Gas temperature at SG U-tube inlet	Averaged temp. of gas with and without mixing volume	Gas temperature without mixing volume
- Length of first node at U-tube inlet	2.6 m	0.3 m
- Temperature difference between gas and wall at first node of U-tube	15 K	200 K
- Calculated principal deposition mechanism	Gravitational settling onto upward facing bend of U-tube	Thermophoresis at U-tube inlet
- Calculated decay heat from deposited FP onto SG U-tube	About 50 W/m^2 1*) (at upward facing bend of U-tube)	About 3,000 W/m^2 (at U-tube inlet)

1*) The value was calculated from the total decay heat in the tubes which is equal to about 0.15 MW/steam generator[7].

6. CONCLUSIONS

The integrity of steam generator U-tube during TMLB' sequence of Surry nuclear plant with and without secondary system depressurization was analyzed with SCDAP/RELAP5/Mod3.1 taking into account the decay heat from deposited FP which was calculated by JAERI's FP aerosol behavior analysis code, ART.

Before that analyses, the RELAP5 model of the hot leg countercurrent natural circulation (CCNC) flow prepared originally by INEEL which plays an important role on the integrity of reactor coolant system structures was validated through the analysis for JAERI's LSTF experiment. The calculation with the INEEL's CCNC model reproduced well the hot leg temperature trends observed in the LSTF countercurrent flow experiment and indicated that the INEEL's model is mostly reliable.

The FP deposition analysis with ART, and the thermohydraulic & structural response analyses with SCDAP/RELAP5 using the hot leg CCNC flow model showed the followings; The ART analysis predicted that a relatively large amount of FPs may deposit on steam generator U-tube inlet mainly by thermophoresis during TMLB' sequences with and without secondary system depressurization. The SCDAP/RELAP5 analyses considering the FP decay heat showed that the steam generator U-tube integrity would be maintained during those sequences because the earliest creep rupture would occur at pressurizer surge line rather than at steam genarator U-tube in both cases. However, the margin for steam generator U-tube integrity during secondary system depressurization was considerably narrower than that without depressurization. Taking into account associated uncertainties in the present analyses, the potential for steam generator tube rupture cannot be ignored. Accordingly, this should be considered in the evaluation of merits and demerits of accident management measures related with the secondary system depressurization.

ACKNOWLEDGMENTS

The present study was performed under the provisions of the agreement between Japan Atomic Energy Research Institute (JAERI) and United States Nuclear Regulatory Commission (USNRC) on the Cooperative Severe Accident Research Program (CSARP). The authors would like to express their sincere appreciation to the late Dr. Y. Chen of USNRC for providing necessary information for the present analyses. Special thanks are also due to Dr. C. Tinkler and Mr. J.

Schaperow of USNRC for discussing the results of present SCDAP/RELAP5 calculations. The authors are grateful to members of the Safety Facility Engineering Services Division for conducting the LSTF experiment and to Mr. E. Ohtani of Nippon Computer Bureau LTD for his calculation of the LSTF experiment with the RELAP5 code.

REFERENCES

1) U. S. Nuclear Regulatory Commission, "Severe Accident Risks: An Assessment for Five U.S. Nuclear Power Plants," NUREG-1150 (1990).
2) D. J. Hansen, et al., "Depressurization as an Accident Management Strategy to Minimize the Consequences of Direct Containment Heating," NUREG/CR-5447 (1990).
3) A. Hidaka, et al., "Severe Accident Management of PWR by an Intentional Primary System Depressurization," JAERI-M 91-175 (in Japanese) (1991).
4) D. L. Knudsen, et al., "Assessment of the Potential for High-Pressure Melt Ejection Resulting from a Surry Station Blackout Transient," NUREG/CR-5949 (1993).
5) M. M. Pilch, et al., "The Probability of Containment Failure by Direct Containment Heating in Surry," NUREG/CR-6109 (1995).
6) E.W. Coryell, et al., "SCDAP/RELAP5/Mod3.1 Code Manual," NUREG/CR-6150 (1995).
7) U. S. Nuclear Regulatory Commission, "Risk Assessment of Severe Accident-Induced Steam Generator Tube Rupture," NUREG-1570 (1998).
8) ROSA-IV Group, "ROSA-IV Large Scale Test Facility (LSTF) System Description," JAERI-M 84-237 (1984).
9) M. Kajimoto, et al., "Development of THALES-2, A Computer Code for Coupled Thermal-Hydraulics and FP Transport Analyses for Severe Accident at LWRs and Its Application to Analysis of FP Revaporization Phenomena," Proc. Int. Topical Meeting on Safety of Thermal Reactors, Portland, pp.584-592 (1991).
10) P. D. Bayless, et al., "Severe Accident Natural Circulation Studies at the INEL," NUREG/CR-6285 (1995).
11) W. A. Stewart, et al., "Natural Circulation Experiments for PWR High Pressure Accidents," EPRI Project No. RP2177-5 (1992).
12) H. M. Domanus, et al., "Analysis of Natural-Convection Phenomena in a 3-Loop PWR during a TMLB' Transient using the COMMIX Codes," NUREG/CR-5070 (1988).
13) A. Hidaka, et al., "SCDAP/RELAP5 Analysis of Station Blackout with Pump Seal LOCA in Surry Plant," J. Nucl. Sci. Technol., Vol.32, No.6, pp.527-538 (1995).

14) V. H. Ransom, et al., "RELAP5 Mod2 Code Manual Volumes 1 and 2," NUREG/CR-4312 (1985).

15) H. Jordan, et al., "TRAP-MELT2 User's Manual," NUREG/CR-4205 (1985).

16) Virginia Power Company, "Surry Power Station Updated Final Safety Analysis Report," Docket 05000280 (1982).

17) F. Gelbard, et al. "Sectional Representations for Simulating Aerosol Dynamics," J. Colloid and Int. Sci., 76, [2], 541 (1980).

18) L. N. Kmetyk, et al., "MELCOR 1.8.2 Assessment: Surry PWR TMLB' (with a DCH Study)," SAND93-1899 (1994).

19) F. R. Larson, et al., "A Time Temperature Relationship for Rupture and Creep Stress," Trans. of the ASME, pp.765-775 (1952).

20) N. E. Bixler, et al., "VICTORIA2.0: A Mechanistic Model for Radionuclide Behavior in a Nuclear Reactor Coolant System Under Severe Accident Conditions," NUREG/CR-6131 (1998).

21) A. Hidaka, et al., "Deposition of Cesium Iodide Particles in Bends and Sections of Vertical Pipe under Severe Accident Conditions," To be published in J. Aerosol Sci. (1999).

Appendix 1 ART Input Data for SG U-tube Integrity (Case 3; without MSRV Bleed)

```
<< ART / SGU Tube >>>:2000secRun
&NDPTIM
    TEND = 2000.0, TSHUT= 12000.0, TEND = 2000.0,
    LPITCH= 500,LPITCH= 5000,
    LOPT(1)=29*0,1,
    LOPT(1)= -1, LOPT(1)= 0,
    LOPT(2)=1000,LOPT(2)=200000,
    LOPT(5)=1000,LOPT(5)=200000,LOPT(9)=5000,LOPT(15)=1,LOPT(15)=0,
    ITURB =1, INUC=1, INUC=2, IDHEAT=4,
    IAGLOM=1, IBROW=1,IGRAV=1,IRISK=0,
    ICOND=1, IUGAS=0,IRESUP(1)=23*0,
    NDX=2, NDY=2, NCOM=23, IELEVE=23, IMCOMP=0,
    CSMASS(1)= 456430.,3*59323.,
    CSMASS(1)= 456430.,3*59323., CSMASS(1)= 1.3912E+07,3*1.8082E+06,
    CSMASS(1)= 1.3912E+07,10*1.8082E+05,2*1.8082E+06,
    CSMASS(1)= 1.3912E+07,2*9.041E+04,9*1.8082E+05,2*1.8082E+06,
    CSMASS(1)= 1.3912E+07,5*3.6164E+04,9*1.8082E+05,2*1.8082E+06,
    CSMASS(1)= 1.3912E+07,10*1.8082E+04,9*1.8082E+05,2*1.8082E+06,
    ICORE(1)=23*0,
    IPIPE(1)=23*1,
    RPIPE(1)= 80.41,12*0.9845,
    RPIPE(1)= 80.41,22*0.9845,
    XLPIPE(1)= 219.4, 3*258.8,
    XLPIPE(1)= 219.4,10*25.88, 2*258.8,
    XLPIPE(1)= 219.4, 2*12.94, 9*25.88, 2*258.8,
    XLPIPE(1)= 219.4, 5*5.176, 9*25.88, 2*258.8,
    XLPIPE(1)= 219.4, 10*2.588, 9*25.88, 2*258.8,
    VCOMP(1)= 4.4555E+06, 3*787.97, 1.0
    VCOMP(1)= 4.4555E+06, 3*921920.,1.0
    VCOMP(1)= 4.4555E+06,10*92192. , 2*921920.,1.0
    VCOMP(1)= 4.4555E+06, 2*46086., 9*92192. , 2*921920.,1.0
    VCOMP(1)= 4.4555E+06, 5*18438., 9*92192. , 2*921920.,1.0
    VCOMP(1)= 4.4555E+06, 10*9219.2, 9*92192. , 2*921920.,1.0
    HCOMP(1)= 219.4,10*25.88, 2*258.8,
    HCOMP(1)= 219.4, 2*12.94, 9*25.88, 2*258.8,
    HCOMP(1)= 219.4, 5*5.176, 9*25.88, 2*258.8,
    HCOMP(1)= 219.4, 10*2.588, 9*25.88, 2*258.8,
    DAW(1)= 505.207, 3*6.1858,
    DAW(1)= 505.207, 3*7237.4,
    DAW(1)= 505.207,13*7237.4,
    DAW(1)= 505.207,22*7237.4,
    IFP(1)= 6, 7,
    RHOM(1) = 4.5100, 3.6750,
    RHOM(1) = 3.7839, 3.7839,
    CC(1,1,1)= 26.733, CC(1,1,2)=178.220,
    CC(1,1,1)= 0.0, CC(1,1,2)=0.0,
```

```
      ICLASS=10,
      ARS(1) = 1.00000E-15,8.00000E-15,6.40000E-14,5.12000E-13,
            4.09600E-12,3.27680E-11,2.62144E-10,2.09715E-09,
            1.67772E-08,1.34218E-07,1.07374E-06,
      FXFILM= 0.49225, FCONX= 1.0, FILM= 0.49225,
      FXFILM= 0.0460 , FCONX= 1.0, FILM= 0.0460,
      ALIMIT= 1.0E-38,
      &END
 &DPTIM NTRNDT=1, TNEXTJ=   2003.0,
      DTALLM= 0.02,  DTB= 0.02,
      DTALLM= 0.01,  DTB= 0.01,
      FDFILM(1)= 40.20, 3*0.49225,
      FDFILM(1)= 40.20,12*0.49225,
      FDFILM(1)= 0.122,22*0.0460,
      SRCJ(1,1,1)=1.0858E-03,SRCJ(1,1,2)=7.23869E-03
      SRCJ(1,1,1)=1.27039,  SRCJ(1,1,2)=8.46927,
      AFJ(1)= 4*0.0,
      AFJ(1)=23*0.0,
      FREVAP(1)=4*1.0,    FUGAS(1)=4*1.0,
      FREVAP(1)=23*1.0,    FUGAS(1)=23*1.0,
      XSJ( 1, 1)=4*1.0000E+00, XSJ( 1, 1)=23*1.0000E+00,
      PMPAJ(1)=23*16.0,
      UGJ(1)= 4*0.0, UGJ(1)= 13*0.0, UGJ(1)= 23*0.0,
      UGASJ(1)= 59.43, 41.13, 39.12, 37.75,
      UGASJ(1)= 59.43, 57.60, 53.94, 50.28, 46.62, 42.96, 41.03, 40.82,
            40.62, 40.42, 40.22, 39.12, 37.75,
      UGASJ(1)= 56.75, 55.03, 51.59, 48.15, 44.71, 41.27, 39.53, 39.49,
            39.45, 39.42, 39.38, 39.17, 38.78,
      UGASJ(1)= 56.75, 55.89, 54.17, 51.59, 48.15, 44.71, 41.27, 39.53,
            39.49, 39.45, 39.42, 39.38, 39.17, 38.78,
      UGASJ(1)= 56.75, 56.40, 55.72, 55.03, 54.34, 53.65, 51.59, 48.15,
            44.71, 41.27, 39.53, 39.49, 39.45, 39.42, 39.38, 39.17, 38.78,
      UGASJ(1)= 56.75, 56.58, 56.23, 55.89, 55.54, 55.20, 54.86, 54.51,
            54.17, 53.82, 53.48, 51.59, 48.15, 44.71, 41.27, 39.53,
            39.49, 39.45, 39.42, 39.38, 39.17, 38.78
      GJ(1, 2, 1)= 180.967, GJ(1, 3, 2)= 122.171,
      GJ(1, 4, 3)= 117.037, GJ(1, 5, 4)= 112.883,
      GJ(1, 2, 1)= 211732., GJ(1, 3, 2)= 142940.,
      GJ(1, 4, 3)= 136933., GJ(1, 5, 4)= 132073.,
      GJ(1, 2, 1)= 211732., GJ(1, 3, 2)= 197973.,
      GJ(1, 4, 3)= 184215., GJ(1, 5, 4)= 170457.,
      GJ(1, 6, 5)= 156698., GJ(1, 7, 6)= 146229.,
      GJ(1, 8, 7)= 142339., GJ(1, 9, 8)= 141738.,
      GJ(1,10, 9)= 141138., GJ(1,11,10)= 140537.,
      GJ(1,12,11)= 139936., GJ(1,13,12)= 136933.,
      GJ(1,14,13)= 132073.,
      GJ(1, 2, 1)= 202171., GJ(1, 3, 2)= 189782.,
      GJ(1, 4, 3)= 177392., GJ(1, 5, 4)= 165003.,
      GJ(1, 6, 5)= 152614., GJ(1, 7, 6)= 143288.,
      GJ(1, 8, 7)= 140088., GJ(1, 9, 8)= 139952.,
```

GJ(1,10, 9)= 139815., GJ(1,11,10)= 139679.,
GJ(1,12,11)= 139542., GJ(1,13,12)= 138860.,
GJ(1,14,13)= 137451.,
GJ(1, 2, 1)= 202171., GJ(1, 3, 2)= 191330.,
GJ(1, 4, 3)= 182038., GJ(1, 5, 4)= 177392.,
GJ(1, 6, 5)= 165003., GJ(1, 7, 6)= 152614.,
GJ(1, 8, 7)= 143288., GJ(1, 9, 8)= 140088.,
GJ(1,10, 9)= 139952., GJ(1,11,10)= 139815.,
GJ(1,12,11)= 139679., GJ(1,13,12)= 139542.,
GJ(1,14,13)= 138860., GJ(1,15,14)= 137451.,
GJ(1, 2, 1)= 202171., GJ(1, 3, 2)= 192260.,
GJ(1, 4, 3)= 184826., GJ(1, 5, 4)= 177392.,
GJ(1, 6, 5)= 169959., GJ(1, 7, 6)= 165588.,
GJ(1, 8, 7)= 177392., GJ(1, 9, 8)= 165003.,
GJ(1,10, 9)= 152614., GJ(1,11,10)= 143288.,
GJ(1,12,11)= 140088., GJ(1,13,12)= 139952.,
GJ(1,14,13)= 139815., GJ(1,15,14)= 139679.,
GJ(1,16,15)= 139542., GJ(1,17,16)= 138860.,
GJ(1,18,17)= 137451.,
GJ(1, 2, 1)= 202171., GJ(1, 3, 2)= 192569.,
GJ(1, 4, 3)= 185755., GJ(1, 5, 4)= 178941.,
GJ(1, 6, 5)= 172127., GJ(1, 7, 6)= 168376.,
GJ(1, 8, 7)= 167688., GJ(1, 9, 8)= 167001.,
GJ(1,10, 9)= 166313., GJ(1,11,10)= 165625.,
GJ(1,12,11)= 164631., GJ(1,13,12)= 177392.,
GJ(1,14,13)= 165003., GJ(1,15,14)= 152614.,
GJ(1,16,15)= 143288., GJ(1,17,16)= 140088.,
GJ(1,18,17)= 139952., GJ(1,19,18)= 139815.,
GJ(1,20,19)= 139679., GJ(1,21,20)= 139542.,
GJ(1,22,21)= 138860., GJ(1,23,22)= 137451.,
TWJ(1)= 737.97, 720.11, 709.41, 701.74,
TWJ(1)= 737.97, 736.18, 732.61, 729.04, 725.47, 721.90, 719.57,
718.50, 717.43, 716.36, 715.29, 709.41, 701.74,
TWJ(1)= 751.04, 753.99, 759.89, 765.78, 771.68, 777.57, 780.37,
780.06, 779.75, 779.45, 779.14, 777.44, 773.04,
TWJ(1)= 751.04, 752.52, 755.46, 759.89, 765.78, 771.68, 777.57,
780.37, 780.06, 779.75, 779.45, 779.14, 777.44, 773.04,
TWJ(1)= 751.04, 751.63, 752.81, 753.99, 755.17, 756.35, 759.89,
765.78, 771.68, 777.57, 780.37, 780.06, 779.75, 779.45,
779.14, 777.44, 773.04,
TWJ(1)= 751.04, 751.34, 751.93, 752.52, 753.11, 753.70, 754.28,
754.87, 755.46, 756.05, 756.64, 759.89, 765.78, 771.68,
777.57, 780.37, 780.06, 779.75, 779.45, 779.14, 777.44, 773.04
TJ(1)= 961.89, 737.31, 719.56, 708.18,
TJ(1)= 961.89, 939.44, 894.52, 849.60, 804.69, 759.77, 736.42,
734.65, 732.87, 731.10, 729.32, 719.56, 708.18,
TJ(1)= 997.35, 976.03, 933.39, 890.75, 848.11, 805.46, 783.92,
783.46, 783.01, 782.55, 782.09, 779.59, 775.41,
TJ(1)= 997.35, 986.69, 965.37, 933.39, 890.75, 848.11, 805.46,
783.92, 783.46, 783.01, 782.55, 782.09, 779.59, 775.41,

```
TJ(1)=  997.35, 993.09, 984.56, 976.03, 967.50, 958.97, 933.39,
     890.75, 848.11, 805.46, 783.92, 783.46, 783.01, 782.55,
     782.09, 779.59, 775.41,
TJ(1)=  997.35, 995.22, 990.95, 986.69, 982.43, 978.16, 973.90,
     969.63, 965.37, 961.10, 956.84, 933.39, 890.75, 848.11,
     805.46, 783.92, 783.46, 783.01, 782.55, 782.09, 779.59, 775.41
TMPARJ(1, 1)=10*961.89,  TMPARJ(1, 2)=10*737.31,
TMPARJ(1, 3)=10*719.56,  TMPARJ(1, 4)=10*708.18,
TMPARJ(1, 1)=10*961.89,  TMPARJ(1, 2)=10*939.44,
TMPARJ(1, 3)=10*894.52,  TMPARJ(1, 4)=10*849.60,
TMPARJ(1, 5)=10*804.69,  TMPARJ(1, 6)=10*759.77,
TMPARJ(1, 7)=10*736.42,  TMPARJ(1, 8)=10*734.65,
TMPARJ(1, 9)=10*732.87,  TMPARJ(1,10)=10*731.10,
TMPARJ(1,11)=10*729.32,  TMPARJ(1,12)=10*719.56,
TMPARJ(1,13)=10*708.18,
TMPARJ(1, 1)=10*997.35,  TMPARJ(1, 2)=10*976.03,
TMPARJ(1, 3)=10*933.39,  TMPARJ(1, 4)=10*890.75,
TMPARJ(1, 5)=10*848.11,  TMPARJ(1, 6)=10*805.46,
TMPARJ(1, 7)=10*783.92,  TMPARJ(1, 8)=10*783.46,
TMPARJ(1, 9)=10*783.01,  TMPARJ(1,10)=10*782.55,
TMPARJ(1,11)=10*782.09,  TMPARJ(1,12)=10*779.59,
TMPARJ(1,13)=10*775.41,
TMPARJ(1, 1)=10*997.35,  TMPARJ(1, 2)=10*986.69,
TMPARJ(1, 3)=10*965.37,  TMPARJ(1, 4)=10*933.39,
TMPARJ(1, 5)=10*890.75,  TMPARJ(1, 6)=10*848.11,
TMPARJ(1, 7)=10*805.46,  TMPARJ(1, 8)=10*783.92,
TMPARJ(1, 9)=10*783.46,  TMPARJ(1,10)=10*783.01,
TMPARJ(1,11)=10*782.55,  TMPARJ(1,12)=10*782.09,
TMPARJ(1,13)=10*779.59,  TMPARJ(1,14)=10*775.41,
TMPARJ(1, 1)=10*997.35,  TMPARJ(1, 2)=10*993.09 ,
TMPARJ(1, 3)=10*984.56,  TMPARJ(1, 4)=10*976.03 ,
TMPARJ(1, 5)=10*967.50,  TMPARJ(1, 6)=10*958.97 ,
TMPARJ(1, 7)=10*933.39,  TMPARJ(1, 8)=10*890.75 ,
TMPARJ(1, 9)=10*848.11,  TMPARJ(1,10)=10*805.46 ,
TMPARJ(1,11)=10*783.92,  TMPARJ(1,12)=10*783.46 ,
TMPARJ(1,13)=10*783.01,  TMPARJ(1,14)=10*782.55 ,
TMPARJ(1,15)=10*782.09,  TMPARJ(1,16)=10*779.59 ,
TMPARJ(1,17)=10*775.41,
TMPARJ(1, 1)=10*997.35,  TMPARJ(1, 2)=10*995.22,
TMPARJ(1, 3)=10*990.95,  TMPARJ(1, 4)=10*986.69,
TMPARJ(1, 5)=10*982.43,  TMPARJ(1, 6)=10*978.16,
TMPARJ(1, 7)=10*973.90,  TMPARJ(1, 8)=10*969.63,
TMPARJ(1, 9)=10*965.37,  TMPARJ(1,10)=10*961.10,
TMPARJ(1,11)=10*956.84,  TMPARJ(1,12)=10*933.39,
TMPARJ(1,13)=10*890.75,  TMPARJ(1,14)=10*848.11,
TMPARJ(1,15)=10*805.46,  TMPARJ(1,16)=10*783.92,
TMPARJ(1,17)=10*783.46,  TMPARJ(1,18)=10*783.01,
TMPARJ(1,19)=10*782.55,  TMPARJ(1,20)=10*782.09,
TMPARJ(1,21)=10*779.59,  TMPARJ(1,22)=10*775.41,
&END
```

Appendix 2 ART Input Data for SG U-Tube Integrity (Case 4; with MSRV Bleed)

```
<< ART / SG U Tube >>>:2000secRun
&NDPTIM
    TEND = 2000.0, TSHUT= 12000.0, TEND = 2000.0,
    LPITCH= 500,LPITCH= 5000,
    LOPT(1)=29*0,1,
    LOPT(1)= -1,
    LOPT(2)=1000,LOPT(2)=200000,
    LOPT(5)=1000,LOPT(5)=200000,LOPT(9)=5000,LOPT(15)=1,LOPT(15)=0,
    ITURB =1, INUC=1, INUC=2, IDHEAT=4,
    IAGLOM=1, IBROW=1,IGRAV=1,IRISK=0,
    ICOND=1, IUGAS=0,IRESUP(1)=23*0,
    NDX=2,  NDY=2,
    NCOM=23,  IELEVE=23,  IMCOMP=0,
    CSMASS(1)= 456430.,3*59323.,
    CSMASS(1)= 456430.,3*59323., CSMASS(1)= 1.3912E+07,3*1.8082E+06,
    CSMASS(1)= 1.3912E+07,10*1.8082E+05,2*1.8082E+06,
    CSMASS(1)= 1.3912E+07,2*9.041E+04,9*1.8082E+05,2*1.8082E+06,
    CSMASS(1)= 1.3912E+07,5*3.6164E+04,9*1.8082E+05,2*1.8082E+06,
    CSMASS(1)= 1.3912E+07,10*1.8082E+04,9*1.8082E+05,2*1.8082E+06,
    ICORE(1)=23*0,
    IPIPE(1)=23*1,
    RPIPE(1)= 80.41,12*0.9845,
    RPIPE(1)= 80.41,22*0.9845,
    XLPIPE(1)= 219.4, 3*258.8,
    XLPIPE(1)= 219.4,10*25.88, 2*258.8,
    XLPIPE(1)= 219.4, 2*12.94, 9*25.88, 2*258.8,
    XLPIPE(1)= 219.4, 5*5.176, 9*25.88, 2*258.8,
    XLPIPE(1)= 219.4, 10*2.588, 9*25.88, 2*258.8,
    VCOMP(1)= 4.4555E+06, 3*787.97, 1.0
    VCOMP(1)= 4.4555E+06, 3*921920.,1.0
    VCOMP(1)= 4.4555E+06,10*92192. , 2*921920.,1.0
    VCOMP(1)= 4.4555E+06, 2*46086., 9*92192. , 2*921920.,1.0
    VCOMP(1)= 4.4555E+06, 5*18438., 9*92192. , 2*921920.,1.0
    VCOMP(1)= 4.4555E+06, 10*9219.2, 9*92192. , 2*921920.,1.0
    HCOMP(1)= 219.4,10*25.88, 2*258.8,
    HCOMP(1)= 219.4, 2*12.94, 9*25.88, 2*258.8,
    HCOMP(1)= 219.4, 5*5.176, 9*25.88, 2*258.8,
    HCOMP(1)= 219.4, 10*2.588, 9*25.88, 2*258.8,
    DAW(1)= 505.207, 3*6.1858,
    DAW(1)= 505.207, 3*7237.4,
    DAW(1)= 505.207,13*7237.4,
    DAW(1)= 505.207,22*7237.4,
    IFP(1)= 6, 7,
    RHOM(1) = 4.5100, 3.6750,
    RHOM(1) = 3.7839, 3.7839,
    CC(1,1,1)= 26.733, CC(1,1,2)=178.220,
    CC(1,1,1)= 0.0, CC(1,1,2)=0.0,
```

```
     ICLASS=10,
     ARS(1) = 1.00000E-15,8.00000E-15,6.40000E-14,5.12000E-13,
          4.09600E-12,3.27680E-11,2.62144E-10,2.09715E-09,
          1.67772E-08,1.34218E-07,1.07374E-06,
     FXFILM= 0.49225, FCONX= 1.0, FILM= 0.49225,
     FXFILM= 0.0460 , FCONX= 1.0, FILM= 0.0460,
     FXFILM= 0.0404 , FCONX= 1.0, FILM= 0.0404,
     ALIMIT= 1.0E-38,
     &END
&DPTIM NTRNDT=1, TNEXTJ=   2003.0,
     DTALLM= 0.02,  DTB= 0.02,
     DTALLM= 0.01,  DTB= 0.01,
     FDFILM(1)= 40.20, 3*0.49225,
     FDFILM(1)= 40.20,12*0.49225,
     FDFILM(1)= 0.122,22*0.0460,
     FDFILM(1)= 0.111,22*0.0404,
     SRCJ(1,1,1)=1.0858E-03,SRCJ(1,1,2)=7.23869E-03
     SRCJ(1,1,1)=1.27039,  SRCJ(1,1,2)=8.46927,
     AFJ(1)= 4*0.0,
     AFJ(1)=23*0.0,
     FREVAP(1)=4*1.0,    FUGAS(1)=4*1.0,
     FREVAP(1)=23*1.0,    FUGAS(1)=23*1.0,
     XSJ( 1, 1)=4*1.0000E+00, XSJ( 1, 1)=23*1.0000E+00,
     PMPAJ(1)=23*16.0,
     UGJ(1)= 4*0.0, UGJ(1)= 13*0.0, UGJ(1)= 23*0.0,
     UGASJ(1)= 59.43, 41.13, 39.12, 37.75,
     UGASJ(1)= 59.43, 57.60, 53.94, 50.28, 46.62, 42.96, 41.03, 40.82,
          40.62, 40.42, 40.22, 39.12, 37.75,
     UGASJ(1)= 56.75, 55.03, 51.59, 48.15, 44.71, 41.27, 39.53, 39.49,
          39.45, 39.42, 39.38, 39.17, 38.78,
     UGASJ(1)= 56.75, 55.89, 54.17, 51.59, 48.15, 44.71, 41.27, 39.53,
          39.49, 39.45, 39.42, 39.38, 39.17, 38.78,
     UGASJ(1)= 56.75, 56.40, 55.72, 55.03, 54.34, 53.65, 51.59, 48.15,
          44.71, 41.27, 39.53, 39.49, 39.45, 39.42, 39.38, 39.17,
          38.78,
     UGASJ(1)= 56.75, 56.58, 56.23, 55.89, 55.54, 55.20, 54.86, 54.51,
          54.17, 53.82, 53.48, 51.59, 48.15, 44.71, 41.27, 39.53,
          39.49, 39.45, 39.42, 39.38, 39.17, 38.78
     UGASJ(1)= 59.43, 59.25, 58.88, 58.52, 58.15, 57.78, 57.42, 57.05,
          56.69, 56.32, 55.95, 53.94, 50.28, 46.62, 42.96, 41.03,
          40.82, 40.62, 40.42, 40.22, 39.12, 37.75
     GJ(1, 2, 1)= 180.967, GJ(1, 3, 2)= 122.171,
     GJ(1, 4, 3)= 117.037, GJ(1, 5, 4)= 112.883,
     GJ(1, 2, 1)= 211732., GJ(1, 3, 2)= 142940.,
     GJ(1, 4, 3)= 136933., GJ(1, 5, 4)= 132073.,
     GJ(1, 2, 1)= 211732., GJ(1, 3, 2)= 197973.,
     GJ(1, 4, 3)= 184215., GJ(1, 5, 4)= 170457.,
     GJ(1, 6, 5)= 156698., GJ(1, 7, 6)= 146229.,
     GJ(1, 8, 7)= 142339., GJ(1, 9, 8)= 141738.,
     GJ(1,10, 9)= 141138., GJ(1,11,10)= 140537.,
```

GJ(1,12,11)= 139936., GJ(1,13,12)= 136933.,
GJ(1,14,13)= 132073.,
GJ(1, 2, 1)= 202171., GJ(1, 3, 2)= 189782.,
GJ(1, 4, 3)= 177392., GJ(1, 5, 4)= 165003.,
GJ(1, 6, 5)= 152614., GJ(1, 7, 6)= 143288.,
GJ(1, 8, 7)= 140088., GJ(1, 9, 8)= 139952.,
GJ(1,10, 9)= 139815., GJ(1,11,10)= 139679.,
GJ(1,12,11)= 139542., GJ(1,13,12)= 138860.,
GJ(1,14,13)= 137451.,
GJ(1, 2, 1)= 202171., GJ(1, 3, 2)= 191330.,
GJ(1, 4, 3)= 182038., GJ(1, 5, 4)= 177392.,
GJ(1, 6, 5)= 165003., GJ(1, 7, 6)= 152614.,
GJ(1, 8, 7)= 143288., GJ(1, 9, 8)= 140088.,
GJ(1,10, 9)= 139952., GJ(1,11,10)= 139815.,
GJ(1,12,11)= 139679., GJ(1,13,12)= 139542.,
GJ(1,14,13)= 138860., GJ(1,15,14)= 137451.,
GJ(1, 2, 1)= 202171., GJ(1, 3, 2)= 192260.,
GJ(1, 4, 3)= 184826., GJ(1, 5, 4)= 177392.,
GJ(1, 6, 5)= 169959., GJ(1, 7, 6)= 165588.,
GJ(1, 8, 7)= 177392., GJ(1, 9, 8)= 165003.,
GJ(1,10, 9)= 152614., GJ(1,11,10)= 143288.,
GJ(1,12,11)= 140088., GJ(1,13,12)= 139952.,
GJ(1,14,13)= 139815., GJ(1,15,14)= 139679.,
GJ(1,16,15)= 139542., GJ(1,17,16)= 138860.,
GJ(1,18,17)= 137451.,
GJ(1, 2, 1)= 202171., GJ(1, 3, 2)= 192569.,
GJ(1, 4, 3)= 185755., GJ(1, 5, 4)= 178941.,
GJ(1, 6, 5)= 172127., GJ(1, 7, 6)= 168376.,
GJ(1, 8, 7)= 167688., GJ(1, 9, 8)= 167001.,
GJ(1,10, 9)= 166313., GJ(1,11,10)= 165625.,
GJ(1,12,11)= 164631., GJ(1,13,12)= 177392.,
GJ(1,14,13)= 165003., GJ(1,15,14)= 152614.,
GJ(1,16,15)= 143288., GJ(1,17,16)= 140088.,
GJ(1,18,17)= 139952., GJ(1,19,18)= 139815.,
GJ(1,20,19)= 139679., GJ(1,21,20)= 139542.,
GJ(1,22,21)= 138860., GJ(1,23,22)= 137451.,
GJ(1, 2, 1)= 211732., GJ(1, 3, 2)= 201069.,
GJ(1, 4, 3)= 193502., GJ(1, 5, 4)= 185935.,
GJ(1, 6, 5)= 178368., GJ(1, 7, 6)= 174090.,
GJ(1, 8, 7)= 173102., GJ(1, 9, 8)= 172113.,
GJ(1,10, 9)= 171125., GJ(1,11,10)= 170137.,
GJ(1,12,11)= 167797., GJ(1,13,12)= 184215.,
GJ(1,14,13)= 170457., GJ(1,15,14)= 156698.,
GJ(1,16,15)= 146229., GJ(1,17,16)= 142339.,
GJ(1,18,17)= 141738., GJ(1,19,18)= 141138.,
GJ(1,20,19)= 140537., GJ(1,21,20)= 139936.,
GJ(1,22,21)= 136933., GJ(1,23,22)= 132073.,
TWJ(1)= 737.97, 720.11, 709.41, 701.74,
TWJ(1)= 737.97, 736.18, 732.61, 729.04, 725.47, 721.90, 719.57,
718.50, 717.43, 716.36, 715.29, 709.41, 701.74,

```
TWJ(1)= 751.04, 753.99, 759.89, 765.78, 771.68, 777.57, 780.37,
     780.06, 779.75, 779.45, 779.14, 777.44, 773.04,
TWJ(1)= 751.04, 752.52, 755.46, 759.89, 765.78, 771.68, 777.57,
     780.37, 780.06, 779.75, 779.45, 779.14, 777.44, 773.04,
TWJ(1)= 751.04, 751.63, 752.81, 753.99, 755.17, 756.35, 759.89,
     765.78, 771.68, 777.57, 780.37, 780.06, 779.75, 779.45,
     779.14, 777.44, 773.04,
TWJ(1)= 751.04, 751.34, 751.93, 752.52, 753.11, 753.70, 754.28,
     754.87, 755.46, 756.05, 756.64, 759.89, 765.78, 771.68,
     777.57, 780.37, 780.06, 779.75, 779.45, 779.14, 777.44,
     773.04
TWJ(1)= 737.97, 737.79, 737.43, 737.07, 736.72, 736.36, 736.00,
     735.64, 735.29, 734.93, 734.57, 732.61, 729.04, 725.47,
     721.90, 719.57, 718.50, 717.43, 716.36, 715.29, 709.41,
     701.74
TJ(1)= 961.89, 737.31, 719.56, 708.18,
TJ(1)= 961.89, 939.44, 894.52, 849.60, 804.69, 759.77, 736.42,
     734.65, 732.87, 731.10, 729.32, 719.56, 708.18,
TJ(1)= 997.35, 976.03, 933.39, 890.75, 848.11, 805.46, 783.92,
     783.46, 783.01, 782.55, 782.09, 779.59, 775.41,
TJ(1)= 997.35, 986.69, 965.37, 933.39, 890.75, 848.11, 805.46,
     783.92, 783.46, 783.01, 782.55, 782.09, 779.59, 775.41,
TJ(1)= 997.35, 993.09, 984.56, 976.03, 967.50, 958.97, 933.39,
     890.75, 848.11, 805.46, 783.92, 783.46, 783.01, 782.55,
     782.09, 779.59, 775.41,
TJ(1)= 997.35, 995.22, 990.95, 986.69, 982.43, 978.16, 973.90,
     969.63, 965.37, 961.10, 956.84, 933.39, 890.75, 848.11,
     805.46, 783.92, 783.46, 783.01, 782.55, 782.09, 779.59,
     775.41
TJ(1)= 961.89, 959.65, 955.16, 950.67, 946.17, 941.68, 937.19,
     932.70, 928.21, 923.72, 919.22, 894.52, 849.60, 804.69,
     759.77, 736.42, 734.65, 732.87, 731.10, 729.32, 719.56,
     708.18
TMPARJ(1, 1)=10*961.89,  TMPARJ(1, 2)=10*737.31,
TMPARJ(1, 3)=10*719.56,  TMPARJ(1, 4)=10*708.18,
TMPARJ(1, 1)=10*961.89,  TMPARJ(1, 2)=10*939.44,
TMPARJ(1, 3)=10*894.52,  TMPARJ(1, 4)=10*849.60,
TMPARJ(1, 5)=10*804.69,  TMPARJ(1, 6)=10*759.77,
TMPARJ(1, 7)=10*736.42,  TMPARJ(1, 8)=10*734.65,
TMPARJ(1, 9)=10*732.87,  TMPARJ(1,10)=10*731.10,
TMPARJ(1,11)=10*729.32,  TMPARJ(1,12)=10*719.56,
TMPARJ(1,13)=10*708.18,
TMPARJ(1, 1)=10*997.35,  TMPARJ(1, 2)=10*976.03,
TMPARJ(1, 3)=10*933.39,  TMPARJ(1, 4)=10*890.75,
TMPARJ(1, 5)=10*848.11,  TMPARJ(1, 6)=10*805.46,
TMPARJ(1, 7)=10*783.92,  TMPARJ(1, 8)=10*783.46,
TMPARJ(1, 9)=10*783.01,  TMPARJ(1,10)=10*782.55,
TMPARJ(1,11)=10*782.09,  TMPARJ(1,12)=10*779.59,
TMPARJ(1,13)=10*775.41,
TMPARJ(1, 1)=10*997.35,  TMPARJ(1, 2)=10*986.69,
```

```
TMPARJ(1, 3)=10*965.37,  TMPARJ(1, 4)=10*933.39,
TMPARJ(1, 5)=10*890.75,  TMPARJ(1, 6)=10*848.11,
TMPARJ(1, 7)=10*805.46,  TMPARJ(1, 8)=10*783.92,
TMPARJ(1, 9)=10*783.46,  TMPARJ(1,10)=10*783.01,
TMPARJ(1,11)=10*782.55,  TMPARJ(1,12)=10*782.09,
TMPARJ(1,13)=10*779.59,  TMPARJ(1,14)=10*775.41,
TMPARJ(1, 1)=10*997.35,  TMPARJ(1, 2)=10*993.09 ,
TMPARJ(1, 3)=10*984.56,  TMPARJ(1, 4)=10*976.03 ,
TMPARJ(1, 5)=10*967.50,  TMPARJ(1, 6)=10*958.97 ,
TMPARJ(1, 7)=10*933.39,  TMPARJ(1, 8)=10*890.75 ,
TMPARJ(1, 9)=10*848.11,  TMPARJ(1,10)=10*805.46 ,
TMPARJ(1,11)=10*783.92,  TMPARJ(1,12)=10*783.46 ,
TMPARJ(1,13)=10*783.01,  TMPARJ(1,14)=10*782.55 ,
TMPARJ(1,15)=10*782.09,  TMPARJ(1,16)=10*779.59 ,
TMPARJ(1,17)=10*775.41,
TMPARJ(1, 1)=10*997.35,  TMPARJ(1, 2)=10*995.22,
TMPARJ(1, 3)=10*990.95,  TMPARJ(1, 4)=10*986.69,
TMPARJ(1, 5)=10*982.43,  TMPARJ(1, 6)=10*978.16,
TMPARJ(1, 7)=10*973.90,  TMPARJ(1, 8)=10*969.63,
TMPARJ(1, 9)=10*965.37,  TMPARJ(1,10)=10*961.10,
TMPARJ(1,11)=10*956.84,  TMPARJ(1,12)=10*933.39,
TMPARJ(1,13)=10*890.75,  TMPARJ(1,14)=10*848.11,
TMPARJ(1,15)=10*805.46,  TMPARJ(1,16)=10*783.92,
TMPARJ(1,17)=10*783.46,  TMPARJ(1,18)=10*783.01,
TMPARJ(1,19)=10*782.55,  TMPARJ(1,20)=10*782.09,
TMPARJ(1,21)=10*779.59,  TMPARJ(1,22)=10*775.41,
TMPARJ(1, 1)=10*961.89,  TMPARJ(1, 2)=10*959.65,
TMPARJ(1, 3)=10*955.16,  TMPARJ(1, 4)=10*950.67,
TMPARJ(1, 5)=10*946.17,  TMPARJ(1, 6)=10*941.68,
TMPARJ(1, 7)=10*937.19,  TMPARJ(1, 8)=10*932.70,
TMPARJ(1, 9)=10*928.21,  TMPARJ(1,10)=10*923.72,
TMPARJ(1,11)=10*919.22,  TMPARJ(1,12)=10*894.52,
TMPARJ(1,13)=10*849.60,  TMPARJ(1,14)=10*804.69,
TMPARJ(1,15)=10*759.77,  TMPARJ(1,16)=10*736.42,
TMPARJ(1,17)=10*734.65,  TMPARJ(1,18)=10*732.87,
TMPARJ(1,19)=10*731.10,  TMPARJ(1,20)=10*729.32,
TMPARJ(1,21)=10*719.56,  TMPARJ(1,22)=10*708.18,
&END
```

This is a blank page.

国際単位系 (SI) と換算表

表 1　SI 基本単位および補助単位

量	名称	記号
長さ	メートル	m
質量	キログラム	kg
時間	秒	s
電流	アンペア	A
熱力学温度	ケルビン	K
物質量	モル	mol
光度	カンデラ	cd
平面角	ラジアン	rad
立体角	ステラジアン	sr

表 2　SI と併用される単位

名称	記号
分，時，日	min，h，d
度，分，秒	°，′，″
リットル	l，L
トン	t
電子ボルト	eV
原子質量単位	u

1 eV = 1.60218 × 10^{-19} J

1 u = 1.66054 × 10^{-27} kg

表 5　SI 接頭語

倍数	接頭語	記号
10^{18}	エクサ	E
10^{15}	ペタ	P
10^{12}	テラ	T
10^{9}	ギガ	G
10^{6}	メガ	M
10^{3}	キロ	k
10^{2}	ヘクト	h
10^{1}	デカ	da
10^{-1}	デシ	d
10^{-2}	センチ	c
10^{-3}	ミリ	m
10^{-6}	マイクロ	μ
10^{-9}	ナノ	n
10^{-12}	ピコ	p
10^{-15}	フェムト	f
10^{-18}	アト	a

表 3　固有の名称をもつ SI 組立単位

量	名称	記号	他の SI 単位による表現
周波数	ヘルツ	Hz	s^{-1}
力	ニュートン	N	$m \cdot kg/s^2$
圧力，応力	パスカル	Pa	N/m^2
エネルギー，仕事，熱量	ジュール	J	N·m
工率，放射束	ワット	W	J/s
電気量，電荷	クーロン	C	A·s
電位，電圧，起電力	ボルト	V	W/A
静電容量	ファラド	F	C/V
電気抵抗	オーム	Ω	V/A
コンダクタンス	ジーメンス	S	A/V
磁束	ウェーバ	Wb	V·s
磁束密度	テスラ	T	Wb/m^2
インダクタンス	ヘンリー	H	Wb/A
セルシウス温度	セルシウス度	℃	
光束	ルーメン	lm	cd·sr
照度	ルクス	lx	lm/m^2
放射能	ベクレル	Bq	s^{-1}
吸収線量	グレイ	Gy	J/kg
線量当量	シーベルト	Sv	J/kg

表 4　SI と共に暫定的に維持される単位

名称	記号
オングストローム	Å
バーン	b
バール	bar
ガル	Gal
キュリー	Ci
レントゲン	R
ラド	rad
レム	rem

1 Å = 0.1 nm = 10^{-10} m

1 b = 100 fm^2 = 10^{-28} m^2

1 bar = 0.1 MPa = 10^5 Pa

1 Gal = 1 cm/s^2 = 10^{-2} m/s^2

1 Ci = 3.7 × 10^{10} Bq

1 R = 2.58 × 10^{-4} C/kg

1 rad = 1 cGy = 10^{-2} Gy

1 rem = 1 cSv = 10^{-2} Sv

（注）

1. 表 1 — 5 は「国際単位系」第 5 版，国際度量衡局 1985 年刊行による。ただし，1 eV および 1 u の値は CODATA の 1986 年推奨値によった。
2. 表 4 には海里，ノット，アール，ヘクタールも含まれているが日常の単位なのでここでは省略した。
3. bar は，JIS では流体の圧力を表わす場合に限り表 2 のカテゴリーに分類されている。
4. EC 閣僚理事会指令では bar，barn および「血圧の単位」mmHg を表 2 のカテゴリーに入れている。

換　算　表

力	N(=10^5 dyn)	kgf	lbf
	1	0.101972	0.224809
	9.80665	1	2.20462
	4.44822	0.453592	1

粘度　1 Pa·s(N·s/m^2) = 10 P(ポアズ)(g/(cm·s))

動粘度　1 m^2/s = 10^4 St(ストークス)(cm^2/s)

圧力	MPa(=10 bar)	kgf/cm^2	atm	mmHg(Torr)	lbf/in^2(psi)
	1	10.1972	9.86923	7.50062 × 10^3	145.038
	0.0980665	1	0.967841	735.559	14.2233
	0.101325	1.03323	1	760	14.6959
	1.33322 × 10^{-4}	1.35951 × 10^{-3}	1.31579 × 10^{-3}	1	1.93368 × 10^{-2}
	6.89476 × 10^{-3}	7.03070 × 10^{-2}	6.80460 × 10^{-2}	51.7149	1

エネルギー・仕事・熱量	J(=10^7 erg)	kgf·m	kW·h	cal(計量法)	Btu	ft·lbf	eV
	1	0.101972	2.77778 × 10^{-7}	0.238889	9.47813 × 10^{-4}	0.737562	6.24150 × 10^{18}
	9.80665	1	2.72407 × 10^{-6}	2.34270	9.29487 × 10^{-3}	7.23301	6.12082 × 10^{19}
	3.6 × 10^6	3.67098 × 10^5	1	8.59999 × 10^5	3412.13	2.65522 × 10^6	2.24694 × 10^{25}
	4.18605	0.426858	1.16279 × 10^{-6}	1	3.96759 × 10^{-3}	3.08747	2.61272 × 10^{19}
	1055.06	107.586	2.93072 × 10^{-4}	252.042	1	778.172	6.58515 × 10^{21}
	1.35582	0.138255	3.76616 × 10^{-7}	0.323890	1.28506 × 10^{-3}	1	8.46233 × 10^{18}
	1.60218 × 10^{-19}	1.63377 × 10^{-20}	4.45050 × 10^{-26}	3.82743 × 10^{-20}	1.51857 × 10^{-22}	1.18171 × 10^{-19}	1

1 cal = 4.18605 J (計量法)

= 4.184 J (熱化学)

= 4.1855 J (15 °C)

= 4.1868 J (国際蒸気表)

仕事率　1 PS (仏馬力)

= 75 kgf·m/s

= 735.499 W

放射能	Bq	Ci
	1	2.70270 × 10^{-11}
	3.7 × 10^{10}	1

吸収線量	Gy	rad
	1	100
	0.01	1

照射線量	C/kg	R
	1	3876
	2.58 × 10^{-4}	1

線量当量	Sv	rem
	1	100
	0.01	1

（86 年 12 月 26 日現在）

EVALUATION OF STEAM GENERATOR U-TUBE INTEGRITY DURING PWR STATION BLACKOUT WITH SECONDARY SYSTEM DEPRESSURIZATION